

The formation of the Milky Way halo and its dwarf satellites; a NLTE-1D abundance analysis. II. Early chemical enrichment

L. Mashonkina^{1,2}, P. Jablonka^{3,4}, T. Sitnova², Yu. Pakhomov², and P. North³

¹ Universitäts-Sternwarte München, Scheinerstr. 1, D-81679 München, Germany
e-mail: lyuda@usm.lmu.de

² Institute of Astronomy, Russian Academy of Sciences, RU-119017 Moscow, Russia
e-mail: lima@inasan.ru

³ Laboratoire d'Astrophysique, Ecole Polytechnique Fédérale de Lausanne (EPFL), Observatoire de Sauvigny, CH-1290 Versoix, Switzerland

⁴ GEPI, Observatoire de Paris, CNRS, Université Paris Diderot, F-92125 Meudon Cedex, France

Received / Accepted

ABSTRACT

We present the non-local thermodynamic equilibrium (NLTE) abundances of up to 10 chemical species in a sample of 59 very metal-poor (VMP, $-4 \leq [\text{Fe}/\text{H}] \lesssim -2$) stars in seven dwarf spheroidal galaxies (dSphs) and in the Milky Way (MW) halo. Our results are based on high-resolution spectroscopic datasets and homogeneous and accurate atmospheric parameters determined in Paper I.

We show that once the NLTE effects are properly taken into account, all massive galaxies in our sample, that is, the MW halo and the classical dSphs Sculptor, Ursa Minor, Sextans, and Fornax, reveal a similar plateau at $[\alpha/\text{Fe}] \approx 0.3$ for each of the α -process elements: Mg, Ca, and Ti. We put on a firm ground the evidence for a decline in α/Fe with increasing metallicity in the Boötes I ultra-faint dwarf galaxy (UFD), that is most probably due to the ejecta of type Ia supernovae. For Na/Fe, Na/Mg, and Al/Mg, the MW halo and all dSphs reveal indistinguishable trends with metallicity, suggesting that the processes of Na and Al synthesis are identical in all systems, independent of their mass. The dichotomy in the [Sr/Ba] versus [Ba/H] diagram is observed in the classical dSphs, similarly to the MW halo, calling for two different nucleosynthesis channels for Sr. We show that Sr in the massive galaxies is well correlated with Mg suggesting a strong link to massive stars and that its production is essentially independent of Ba, for most of the [Ba/H] range. Our three UFDs, that is Boötes I, UMa II, and Leo IV, are depleted in Sr and Ba relative to Fe and Mg, with very similar ratios of [Sr/Mg] ≈ -1.3 and [Ba/Mg] ≈ -1 on the entire range of their Mg abundances. The subsolar Sr/Ba ratios of Boötes I and UMa II indicate a common r-process origin of their neutron-capture elements. Sculptor remains the classical dSph, in which the evidence for inhomogeneous mixing in the early evolution stage, at $[\text{Fe}/\text{H}] < -2$, is the strongest.

Key words. Line: formation – Nuclear reactions, nucleosynthesis, abundances – Stars: abundances – Galaxies: abundances – Local Group – Galaxies: dwarf

1. Introduction

We aim at understanding the physical conditions at the onset of star formation in galaxies. The stellar abundance trends and dispersions of the most metal-poor stars reveal the nature of the first generations of stars (e.g., mass, numbers, spatial distribution), and the level of homogeneity of the primitive interstellar medium (e.g., size/mass of star forming regions, nature and energetics of the explosion of supernovae). The proximity of the Local Group dwarf spheroidal galaxies (dSphs) allows the derivation of chemical abundances with comparable quality as in the Milky Way (MW). The comparison of these galaxies with very different masses, star formation histories, and level of chemical enrichment can bring crucial information on the universality of the physical processes at play. This type of comparative analyses is at the frontier fields between stellar and galaxy evolution, as for example, it provides a very detailed testbed for the Λ CDM paradigm, improves our understanding of fundamental parameters, such as the sampling of the initial mass function, but also provides most wanted constraints on the nucleosynthetic origin of still puzzling categories of chemical species, such as

the neutron-capture elements or the odd-nuclear charge (odd- Z) elements sodium and aluminum.

As a consequence of their distance, most of the stars accessible in dSphs at high spectral resolution are giants. Low total gas pressure and low electron number density lead to departures from local thermodynamical equilibrium (LTE) in their atmospheres, while the non-local thermodynamical equilibrium (NLTE) line formation impacts each chemical species differently, in magnitude and sign, depending on the stellar atmosphere parameters and element abundances (for review, see Asplund 2005, Mashonkina 2014). Therefore, ignoring the NLTE effects for stellar samples covering broad metallicity ranges can lead to a distorted picture of the galactic abundance trends.

This paper is the second part of a project aiming at providing a homogeneous set of NLTE elemental abundances for the very and extremely metal-poor (VMP: $[\text{Fe}/\text{H}]^1 \leq -2$, EMP: $[\text{Fe}/\text{H}] \leq -3$) stars both in the Local Group dwarf spheroidal galaxies and in the halo of the Milky Way. Accurate atmospheric param-

Send offprint requests to: L. Mashonkina; e-mail: lima@inasan.ru

¹ In the classical notation, where $[\text{X}/\text{H}] = \log(N_{\text{X}}/N_{\text{H}})_{\text{star}} - \log(N_{\text{X}}/N_{\text{H}})_{\text{sun}}$.

eters for our stellar sample were derived in our previous study (Mashonkina et al. 2017, hereafter, Paper I).

Our work has been preceded by a number of important efforts to evaluate the NLTE effects on determination of chemical abundances for late-type stars.

For the chemical species of our interest in the metallicity range similar to that of our study, from extremely to very metal-poor stars, the NLTE abundance corrections were calculated for Na I (Baumueller et al. 1998, Mashonkina et al. 2000, Andrievsky et al. 2007), Mg I (Idiart & Thévenin 2000, Shimanskaya et al. 2000, Zhao & Gehren 2000, Andrievsky et al. 2010), Al I (Baumueller & Gehren 1997, Andrievsky et al. 2008), Si I (Shi et al. 2009), Ca I (Idiart & Thévenin 2000, Mashonkina et al. 2007, Spite et al. 2012), Ti I-Ti II (Bergemann 2011, Sitnova 2016), Sr II (Mashonkina & Gehren 2001, Andrievsky et al. 2011, Bergemann et al. 2012), and Ba II (Mashonkina et al. 1999, Andrievsky et al. 2009). Recently, Zhao et al. (2016) derived the NLTE abundances of a wealth of elements, from Li to Eu, for a sample of 51 Galactic dwarf stars covering the $-2.6 \leq [\text{Fe}/\text{H}] \leq 0.2$ range. They have the closest methodology to the present study, and are complementary in the spectral type of stars as well as the metallicity range.

Since in most cases, the departures from LTE for individual lines depend strongly on the stellar atmosphere parameters and elemental abundances, we do not use pre-existing NLTE abundance corrections from the literature. Instead, the NLTE calculations are performed for each star and chemical species. Our approach stands out among the previous publications by three specific features at least: i) the $[\text{X}/\text{Fe}]$ abundance ratios are calculated by correcting the iron abundances from NLTE effects as well, unlike most of our predecessors; ii) the NLTE abundances are calculated in idem homogeneous way for all elements; iii) we go beyond the Milky Way stellar population and address the chemical trends of the Local Group dwarf spheroidal galaxies.

In the following, Sect. 2 briefly describes our stellar sample, the observational material, and the adopted method to derive the atmospheric parameters. Details of the NLTE calculations and the abundance determinations, including atomic models, line list, and codes, are provided in Sect. 3. Section 4 details the impact of the NLTE treatment on each individual chemical species, while Sect. 5 presents the abundance trends within each galaxy and draws comparisons between them to infer their chemical evolution. It also provides new constrains on the nucleosynthetic origin of the neutron-capture elements. Our results are summarized in Sect. 6.

2. Stellar sample, observational material, and atmospheric parameters

Our stellar sample, the observational material, and the determination of atmospheric parameters were described in Paper I. We summarize below the main features.

Sample. We are working with two stellar samples of cool giants in the $-4 \lesssim [\text{Fe}/\text{H}] \lesssim -2$ metallicity range. One is composed of 23 stars in the Milky Way halo, the other encompasses 36 stars in a number of MW satellites, namely, the classical dSphs Sculptor (Scl), Ursa Minor (UMi), Fornax (Fnx), and Sextans (Sex) and the ultra-faint dwarfs (UFDs) Boötes I, UMa II, and Leo IV.

Material. Each star was observed at high spectral resolution, $R = \lambda/\Delta\lambda \geq 25\,000$. We used the stellar spectra from public and private archives as well as published equivalent widths.

Stellar atmosphere parameters. We used a combination of photometric and spectroscopic methods to derive a homoge-

neous set of stellar atmosphere parameters: effective temperature T_{eff} , surface gravity $\log g$, iron abundance $[\text{Fe}/\text{H}]$, and microturbulence velocity ξ_t . Our spectroscopic analyses take advantage of NLTE line formation.

For both stellar samples we rely on photometric effective temperatures. The surface gravities of the dSph stars were calculated by applying the standard relation between $\log g$, T_{eff} , the absolute bolometric magnitude, and the stellar mass, that was assumed to be $0.8 M_{\odot}$. The Fe I- and Fe II-based NLTE abundances of the dSph stars are fully consistent in the $[\text{Fe}/\text{H}] > -3.7$ regime. We therefore applied the Fe I/Fe II ionisation equilibrium method to determine the surface gravities of the MW giants, for which distances are mostly unknown or inaccurate. The abundance difference between Fe I and Fe II does not exceed 0.12 dex and 0.06 dex for the dSph and MW stars, respectively.

We noted that the NLTE treatment fails to achieve consistent abundances from Fe I and Fe II in the most metal-poor ($[\text{Fe}/\text{H}] < -3.7$) stars in the dSphs. In consequence, we did not enforce the Fe I/Fe II ionisation equilibrium for the most metal-poor star in the MW comparison sample, HE1357-0123 ($[\text{Fe}/\text{H}] \simeq -3.9$), but used an upward revised, by 0.2 dex, $\log g$ derived by Cohen et al. (2013) from the isochrone method.

The problem of the Fe I/Fe II ionisation equilibrium of our most metal-poor stars most probably relates to the uncertainty in the photometric calibration of T_{eff} at these extremely low metallicities. Hence, our final $[\text{Fe}/\text{H}]$ values, for the entire sample, are based on lines of Fe II only.

Our sample stars and their atmospheric parameters are listed in Table 1.

3. Method

3.1. NLTE calculations

The present investigation is based on the NLTE methods developed in our earlier studies and documented in a number of papers (see Table 2 for the refereces), in which the atomic data and the questions of line formation have been considered in detail. We have updated collisional data for a number of chemical species. For Sr II we apply here the electron-impact excitation rate coefficients from *ab initio* calculations of Bautista et al. (2002). For Al I, Si I, and Ca I, the inelastic collisions with neutral hydrogen particles are treated using the accurate rate coefficients from quantum-mechanical calculations of Belyaev (2013), Belyaev et al. (2014), and Belyaev et al. (2016), respectively. For Ti I-II, Fe I-II, Sr II, and Ba II we rely on the Drawin (1968) approximation, as implemented by Steenbock & Holweger (1984), and apply a scaling factor S_{H} to the Drawinian rates. The magnitude of S_{H} indicated in Table 2 was estimated empirically for every chemical species in our earlier papers.

To solve the coupled radiative transfer and statistical equilibrium (SE) equations, we employed a revised version of the DETAIL code (Butler & Giddings 1985) based on the accelerated lambda iteration method, as described in Rybicki & Hummer (1991, 1992). An update of the opacity package in DETAIL was presented by Mashonkina et al. (2011).

3.2. Line selection, atomic data, and notes on abundance determinations

The spectral lines used in the abundance analysis are listed in Table 3 together with their atomic parameters. The *gf*-values are taken from VALD3, with the exception of Fe II, for which we used *gf*-values from Raassen & Uylings (1998) that were

Table 1. Atmospheric parameters of the investigated sample.

ID	$T_{\text{eff}}[\text{K}]$	$\log g$	[Fe/H]	$\xi_t[\text{km s}^{-1}]$
ScI ET0381	4570	1.17	-2.19	1.7
ScI002_06	4390	0.68	-3.11	2.3
ScI03_059	4530	1.08	-2.88	1.9
ScI031_11	4670	1.13	-3.69	2.0
ScI074_02	4680	1.23	-3.06	2.0
ScI07-49	4630	1.28	-2.99	2.0
ScI07-50	4800	1.56	-4.00	2.2
ScI11_1_4296	4810	1.76	-3.70	1.9
ScI6_6_402	4890	1.78	-3.66	1.8
ScI S1020549	4650	1.35	-3.67	2.0
ScI1019417	4280	0.50	-2.48	2.0
Fnx05-42	4350	0.70	-3.37	2.3
Sex11-04	4380	0.57	-2.60	2.2
Sex24-72	4400	0.76	-2.84	2.2
UMi396	4320	0.70	-2.26	2.5
UMi446	4600	1.37	-2.52	2.5
UMi718	4630	1.13	-2.00	2.0
UMi COS233	4370	0.77	-2.23	2.0
UMi JI19	4530	1.00	-3.02	2.0
UMi20103	4780	1.55	-3.09	2.0
UMi28104	4275	0.65	-2.12	2.0
UMi33533	4430	0.75	-3.14	2.0
UMi36886	4400	0.82	-2.56	2.0
UMi41065	4350	0.63	-2.48	2.0
Boo-033	4730	1.4	-2.26	2.3
Boo-041	4750	1.6	-1.54	2.0
Boo-094	4570	1.01	-2.69	2.2
Boo-117	4700	1.4	-2.09	2.3
Boo-127	4670	1.4	-1.93	2.3
Boo-130	4730	1.4	-2.20	2.3
Boo-980	4760	1.8	-2.94	1.8
Boo-1137	4700	1.39	-3.76	1.9
UMa II-S1	4850	2.05	-2.96	1.8
UMa II-S2	4780	1.83	-2.94	2.0
UMa II-S3	4560	1.34	-2.26	1.8
Leo IV-S1	4530	1.09	-2.58	2.2
HD 2796	4880	1.55	-2.32	1.8
HD 4306	4960	2.18	-2.74	1.3
HD 8724	4560	1.29	-1.76	1.5
HD 108317	5270	2.96	-2.18	1.2
HD 122563	4600	1.32	-2.63	1.7
HD 128279	5200	3.00	-2.19	1.1
HD 218857	5060	2.53	-1.92	1.4
HE0011-0035	4950	2.0	-3.04	2.0
HE0039-4154	4780	1.6	-3.26	2.0
HE0048-0611	5180	2.7	-2.69	1.7
HE0122-1616	5200	2.65	-2.85	1.8
HE0332-1007	4750	1.5	-2.89	2.0
HE0445-2339	5165	2.2	-2.76	1.9
HE1356-0622	4945	2.0	-3.45	2.0
HE1357-0123	4600	1.2	-3.92	2.1
HE1416-1032	5000	2.0	-3.23	2.1
HE2244-2116	5230	2.8	-2.40	1.7
HE2249-1704	4590	1.2	-2.94	2.0
HE2252-4225	4750	1.55	-2.76	1.9
HE2327-5642	5050	2.20	-2.92	1.7
BD -11° 0145	4900	1.73	-2.18	1.8
CD -24° 1782	5140	2.62	-2.72	1.2
BS16550-087	4750	1.5	-3.33	2.0

Table 2. Atomic models used in this study.

Species	Reference	H I collisions
Na I	Alexeeva et al. (2014)	BBD10
Mg I	Mashonkina (2013)	BBS12
Al I	Baumüller & Gehren (1996)	B13
Si I	Shi et al. (2008)	BYB14
Ca I-II	Mashonkina et al. (2007)	BYG16
Ti I-II	Sitnova et al. (2016)	$S_{\text{H}} = 1$
Fe I-II	Mashonkina et al. (2011)	$S_{\text{H}} = 0.5$
Sr II	Belyakova & Mashonkina (1997)	$S_{\text{H}} = 0.01$
Ba II	Mashonkina et al. (1999)	$S_{\text{H}} = 0.01$
Eu II	Mashonkina & Gehren (2000)	$S_{\text{H}} = 0.1$

Notes. Collisions with H I are treated following to

BBD10 = Barklem et al. (2010),

BBS12 = Barklem et al. (2012),

B13 = Belyaev (2013), BYB14 = Belyaev et al. (2014),

BYG16 = Belyaev et al. (2016),

Steenbock & Holweger (1984), with a scaling factor of S_{H} .

corrected by +0.11 dex, following the recommendation of Grevesse & Sauval (1999). The van der Waals broadening was accounted for by applying accurate data based on the perturbation theory (see Barklem et al. 2000, and references therein), with the exception of Ca I, for which we employed the van der Waals damping constants, Γ_6 , based on laboratory measurements of Smith (1981), and a few selected lines of Na I, Al I, Mg I, and Ba II, for which Γ_6 was estimated empirically from solar line-profile fitting by Gehren et al. (2004, Na I and Al I), Mashonkina (2013, Mg I), and Mashonkina et al. (2008, Ba II).

In VMP stars, aluminum can only be observed in the resonance doublet lines Al I 3944 and 3961 Å located in the spectral range that is crowded even at so low metallicity and rather noisy, in particular, in case of the dSph stars. The Al I 3944.006 Å line is heavily blended by the molecular CH 3943.85 and 3944.16 Å lines, and it was only used for an EMP star ScI031_11, which has low carbon abundance (Jablonka et al. 2015) and the best-quality observed spectrum. The second line, Al I 3961 Å, lies in the wing of Ca II 3968 Å and must be synthesised with a pre-determined calcium abundance.

For the Si abundance determination, we prefer to employ Si I 4102 Å, which lies in the far wing of H δ , but not affected by any other atomic or molecular lines. However, for 9 stars in the dSphs and 12 MW stars with the best-quality spectra we use also Si I 3905.52 Å. This line is blended by the molecular CH 3905.68 Å line, and the Si abundance was derived either via spectral synthesis (six dSph stars) or by estimating a contribution of the CH line to the 3905 Å blend via spectral synthesis. The C/Fe abundance ratios were taken from Cohen & Huang (2010), Norris et al. (2010), Tafelmeyer et al. (2010), Cohen et al. (2013), and Jablonka et al. (2015). Our analysis of the CH 4310 Å band in the available spectra has confirmed the literature data on [C/Fe]. It is worth noting that the investigated dSph stars have low carbon abundance, with [C/Fe] ≤ 0 . The exception is Boo-1137, with [C/Fe] = 0.25 (Norris et al. 2010). We evaluated the difference in the Si abundance derived without and with the CH line taken into account. For Boo-1137 it amounts to 0.32 dex. The stars of the MW comparison sample were preselected by requiring [C/Fe] ≤ 0 .

The best observed neutron-capture elements are strontium and barium. Unfortunately, even their abundances are not al-

ways accessible in our MW and dSph sample stars. This is partly because the observations did not cover the strongest lines of these elements located in the blue spectral range and partly because some spectra are too noisy in these regions. For example, Sr II 4077, 4215 Å are missing in the Boötes I spectra of Gilmore et al. (2013) and so are the Sr II and Ba II resonance lines in Scl07-49, HD 218857, and CD-24°1782. For several stars, the resonance lines of Sr II and/or Ba II could not be extracted from noise. This is the case of five stars in the Sculptor dSph, that is, 11_1_4296 and S1020549 from Simon et al. (2015) and 002_06, 031_11, and 074_02 from Jablonka et al. (2015), and a MW halo star HE1357-0123 from Cohen et al. (2013). We caution that we could not use the Ba II equivalent widths of Ural et al. (2015) as a consequence of strong inconsistencies between lines. For example, in UMi718, Ural et al. (2015) measured $W_{obs} = 63.5$ mÅ for Ba II 5853 Å ($E_{exc} = 0.6$ eV, $\log gf = -1$), while $W_{obs} = 28.8$ mÅ for Ba II 6496 Å ($E_{exc} = 0.6$ eV, $\log gf = -0.38$). For Ba II 4554 Å ($E_{exc} = 0$, $\log gf = 0.17$) in UMi446, they give $W_{obs} = 72.1$ mÅ, but larger value of $W_{obs} = 144.4$ mÅ for Ba II 6496 Å.

For Sr II, we attempted to use both resonance lines when they are available. The Sr II 4215.539 Å line is notably blended by Fe I 4215.426 Å in the $[Fe/H] > -3$ stars and therefore was ignored in the abundance analysis, if Sr II 4077 Å was available. The case of Boo-127 ($[Fe/H] = -1.93$) makes an exception to this rule. As in Frebel et al. (2016), the synthetic spectrum analysis results in a substantially lower abundance from Sr II 4077 Å, by 0.5 dex, compared with that from Sr II 4215 Å. The Sr abundance of Boo-127 was derived from Sr II 4215 Å.

The Ba II 4934 Å and 6141 Å lines are blended with some Fe I lines (see details in Jablonka et al. 2015). Whenever the spectrum was available, the Ba abundance was determined from spectral synthesis. Otherwise, the contribution of the Fe I lines to the blends at 4934 Å and 6141 Å was estimated by computing their synthetic spectra. When the blending between the Fe and Ba lines was substantial, then Ba II 6141 Å was not used.

The lines of Sr II, Ba II, and Eu II are composed of multiple components because each of these chemical elements is represented by several isotopes. For Sr II 4077 and 4215 Å, their isotopic splitting (IS) and hyper-fine splitting (HFS) structure is taken into account using the atomic data from Borghs et al. (1983) and the solar system Sr isotope abundance ratios from Lodders et al. (2009). It is worth noting that the difference between the solar system and the r-process Sr isotope mixture (Arlandini et al. 1999) produces negligible effect on the derived stellar Sr abundances.

In contrast, the Ba abundance derived from the 4554 Å and 4934 Å resonance lines depends on the isotope mixture adopted in the calculations because of substantial separations of 57 and 78 mÅ, respectively, between the HFS components (Brix & Kopfermann 1952, Silverans et al. 1980, Blatt & Werth 1982, Becker & Werth 1983). Since the odd-*A* isotopes ^{135}Ba and ^{137}Ba have very similar HFS, the abundance is essentially dependent on the total fractional abundance of these odd isotopes, f_{odd} . The larger f_{odd} , the broader the resonance line is, and the larger energy it absorbs. In the Solar system matter, $f_{odd} = 0.18$ (Lodders et al. 2009), however, larger value of $f_{odd} = 0.438$ (Kratz et al. 2007) to 0.72 (McWilliam 1998) is predicted for pure r-process production of barium. We inspected the influence of the f_{odd} variation on the Ba abundance determinations. In the four MW stars, with $W_{obs}(4554 \text{ Å}) \leq 33$ mÅ, the abundance derived from the Ba II resonance line is, in fact, insensitive to the

adopted f_{odd} value. In Boo-1137, with $W_{obs}(4934 \text{ Å}) = 40.5$ mÅ, and Leo IV-S1, with $W_{obs}(4554 \text{ Å}) = 62$ mÅ, the abundance difference between using $f_{odd} = 0.18$ and 0.46 amounts to $\Delta \log \varepsilon = 0.03$ dex and 0.05 dex, respectively. A notable shift of $\Delta \log \varepsilon = 0.18$ dex was only found for HE0011-0035, with $W_{obs}(4554 \text{ Å}) = 104$ mÅ.

Fortunately, the Ba II 5853, 6141, and 6497 Å subordinate lines are almost free of HFS effects. Therefore, in case the subordinate lines are available, they were used to derive the Ba abundance, at the exception of Boo-1137, for which Ba II 6141 and 6497 Å are rather weak. No subordinate line could be measured for Leo IV-S1, HE0011-0035, HE0122-1616, HE1356-0622, HE1416-1032, HE2249-1704, and BS16550-087, and the Ba abundance was determined from the resonance lines, adopting $f_{odd} = 0.46$, as predicted by Travaglio et al. (1999) for the r-process Ba isotope mixture.

We could determine the Eu abundances for six dSph stars and 12 MW halo stars. For eight of them, we work on the observed spectra and perform spectral synthesis of the Eu II lines. For the other stars, we use the equivalent widths published by Kirby & Cohen (2012, Scl 1019417), Cohen & Huang (2010, UMi 28104, 33533, 36886, 41065, and J119), and Cohen et al. (2013, four MW stars). For all, we properly account for the HFS and IS structure thanks to the data of Lawler et al. (2001).

3.3. Codes and model ingredients

In this study, the synthetic spectrum method is used to derive the element abundances from Al I 3944, 3961 Å, Si I 3905, 4102 Å, Sr II 4215 Å, and Ba II 6141 Å to take into account the blending lines and from Ba II 4934, 4554 Å to take into account HFS structure of the lines. For this we used the codes SIU (Reetz 1991) and SYNTHV_NLTE (Ryabchikova et al. 2016) that implement the pre-computed departure coefficients, $b_i = n_i^{NLTE}/n_i^{LTE}$, to calculate the NLTE line profiles for the NLTE species. Here, n_i^{NLTE} and n_i^{LTE} are the statistical equilibrium and thermal (Saha-Boltzmann) number densities, respectively, from DETAIL. The code SYNTHV_NLTE is integrated within the IDL BINMAG3² code, written by O. Kochukhov, finally allowing the user to determine the best fit to the observed line profile. Line list for spectral synthesis has been extracted from the Vienna Atomic Line Database³ (VALD3, Ryabchikova et al. 2015). Our test calculations with the solar model atmosphere in a broad wavelength range (4209 Å to 9111 Å) have proved that using two different codes, SIU and SYNTHV_NLTE + BINMAG3, does not produce systematic shifts in derived abundances, namely, the abundance difference nowhere exceeds 0.03 dex.

For all other lines we use their equivalent widths. For each line, we first calculate the LTE abundance with the code WIDTH9⁴ (Kurucz 2005, modified by Vadim Tsymbal, private communication). The NLTE abundance is then obtained by applying the NLTE abundance correction, $\Delta_{NLTE} = \log \varepsilon_{NLTE} - \log \varepsilon_{LTE}$, computed with the code LINEC (Sakhibullin 1983) that uses the LTE and NLTE level populations from DETAIL. Our test calculations with LINEC and WIDTH9 have proved that, for any given line, both codes lead to consistent LTE abundances within 0.01-0.02 dex.

In a similar homogeneous way, all the codes we used do treat continuum scattering correctly; i.e., scattering is taken into ac-

² <http://www.astro.uu.se/~oleg/download.html>

³ <http://vald.astro.univie.ac.at/vald3/php/vald.php>

⁴ <http://kurucz.harvard.edu/programs/WIDTH/>

count not only in the absorption coefficient, but also in the source function.

As in Paper I, we use the MARCS model structures (Gustafsson et al. 2008).

4. Stellar element abundances

The LTE and NLTE abundances of Na, Mg, Al, Si, Ca, Ti, Ni (only LTE), Sr, and Ba were determined for each star, provided the corresponding lines could be measured. The obtained results are available as online material (Table 3). Other chemical species measured in Jablonka et al. (2015), namely, Sc II, Cr I, Mn I, Co I, and Y II, are absent in our list, because no NLTE calculations were performed in the literature for the atmospheric parameters of our interest.

4.1. Impact of NLTE on derived chemical abundances

Our NLTE calculations for Na I, Mg I, Al I, Si I, Ca I-II, Ti I-II, Fe I-II, Sr II, and Ba II show that the departures from LTE are different for each species, and, in general, depend on the stellar atmosphere parameters and the element abundances. We stress that our procedure consistently accounts for both statistical equilibrium and radiative transfer: the SE (NLTE) calculations were iterated by varying the element abundance until agreement was reached between the resulting model spectra and the observed ones. Figure 1 displays the differences between the average NLTE and LTE abundance, (NLTE - LTE), for the individual stars. It is worth noting that this difference is set to the NLTE abundance correction, Δ_{NLTE} , if we have one line, for example, for Al I and Si I.

We discuss different NLTE species by separating them depending on the dominant NLTE mechanism, but not in the order of their nuclear charge. The NLTE effects for Ti I and Fe I were described in our Paper I. For the reader convenience, we show the NLTE - LTE abundance differences for Ti I and Fe I also in this paper (Fig. 1). For the range of stellar atmosphere parameters investigated in this study, all the NLTE neutral species are minority ones. For example, even Si I, which has the largest ionisation energy, $E_{\text{ion}} = 8.15$ eV, contributes about 10 % to the total Si abundance in the line-formation layers of the model with $T_{\text{eff}}/\log g/[\text{Fe}/\text{H}] = 4590/1.20/-2.9$. The number density of these minority species easily deviates from thermodynamic equilibrium, when the intensity of the ionising radiation deviates from the Planck function.

As discussed in the NLTE papers referenced in Table 2, the main NLTE mechanism for Mg I, Al I, and Ca I is the ultra-violet (UV) over-ionisation. It results in the depletion of the atomic level populations and weakened spectral lines compared to the LTE case and thus in positive NLTE corrections.

4.1.1. Al I

The largest positive NLTE corrections are computed for the resonance lines of Al I. For example, $\Delta_{\text{NLTE}}(\text{Al I } 3961 \text{ \AA})$ reaches 0.66 dex for Sc16_6_402 (4890/1.78/-3.66). The NLTE effects for Al I depend strongly on stellar T_{eff} , $\log g$, and metallicity (Al abundance), resulting in much larger dispersion of the abundance differences between NLTE and LTE at fixed $[\text{Fe}/\text{H}]$ compared with that for the other species, as shown in Fig. 1. For example, the MW stars HE1356-0622 (4945/2.0/-3.45) and HE1416-1032 (5000/2.0/-3.23) have larger $\Delta_{\text{NLTE}}(\text{Al I } 3961 \text{ \AA})$, by about 0.3 dex, compared with that for the stars of similar metallicity,

but lower effective temperature BS16550-087 (4750/1.5/-3.40) and HE0039-4154 (4780/1.6/-3.26).

4.1.2. Ca I

There is a clear metallicity trend of the NLTE effects for Ca I, with NLTE-LTE approaching 0.3 dex, when $[\text{Fe}/\text{H}]$ is close to -4 . A thorough discussion of the NLTE abundance corrections for an extended list of the Ca I lines can be found in Mashonkina et al. (2016).

We encountered a problem with the Ca I 4226 Å resonance line that gives a lower abundance than the subordinate lines. For example, for Sc1031_11 (4670/1.13/-3.69), the abundance difference between Ca I 4226 Å and three subordinate lines amounts to $\Delta \log \epsilon = -0.65$ in the LTE calculations and becomes even more negative (-0.87 dex) in NLTE. Mashonkina et al. (2007) have first reported a similar case for the $[\text{Fe}/\text{H}] \simeq -2$ dwarf stars, although with a smaller abundance difference. This problem was highlighted by Spite et al. (2012) for their sample of VMP giants and dwarfs. Our calculations show that, in the VMP atmospheres, the total NLTE effect is smaller for the resonance line than for the subordinate ones. Overall over-ionisation of Ca I in deep atmospheric layers leads to weakened subordinate lines and also line wings of Ca I 4226 Å. However, the core of Ca I 4226 Å forms in the uppermost atmospheric layers, where the departure coefficient of the upper level drops rapidly due to photon escape from the line itself, resulting in dropping the line source function below the Planck function and enhanced absorption in the line core. This compensates in part or fully the NLTE effects in the line wings. For example, in the 4670/1.13/-3.69 model, Ca I 4226 Å has equal equivalent widths in NLTE and LTE.

In consequence of the above considerations, we did not use Ca I 4226 Å for the abundance determinations. For Sc107-50 ($[\text{Fe}/\text{H}] = -4.0$), Sc16_6_402 ($[\text{Fe}/\text{H}] = -3.66$), and Sc111_1_4296 ($[\text{Fe}/\text{H}] = -3.7$), their Ca abundance is derived from Ca II 3933 Å. It is worth noting, $\Delta \log \epsilon(\text{Ca II } 3933 \text{ \AA} - \text{Ca I } 4226 \text{ \AA})$ in these stars amounts to 0.59 dex, 0.15 dex, and 0.27 dex, respectively.

4.1.3. Mg I

As can be seen in Fig. 1, NLTE-LTE is mostly positive for Mg I. However, it is negative for Sc107-49 and Fnx05-42, where only the Mg Ib lines could be employed, and for the $[\text{Fe}/\text{H}] > -2.4$ stars, for which the used Mg I 4703 Å and 5528 Å lines are strong ($W_{\text{obs}} > 100 \text{ m\AA}$). Strengthening the Mg Ib lines as compared to the LTE case was discussed in detail by Mashonkina (2013) in her analysis of HD 122563. The case is the same as that of Ca I 4226 Å reported in the previous subsection. We find that similar NLTE mechanisms act for Mg I 4703 Å and 5528 Å, when they are strong. Due to competing NLTE mechanisms, NLTE-LTE for Mg I is overall small, less than 0.12 dex in absolute value, except for Sc107-50 and Sc111_1_4296, for which all the Mg I lines are weak and form in deep atmospheric layers being subject to an over-ionisation of Mg I.

We note that, for Mg I, NLTE leads to smaller line-to-line scatter compared to the LTE case and cancels much of the scatter in $[\text{Mg}/\text{Fe}]$ between stars of close metallicities. Hereafter, the sample standard deviation, $\sigma_{\log \epsilon} = \sqrt{\sum(\bar{x} - x_i)^2/(N_I - 1)}$, determines the dispersion in the single line measurements around the mean. For example, $\sigma_{\log \epsilon} = 0.06$ dex in LTE and 0.03 dex in NLTE for HD 218857 (three lines of Mg I), and the abundance

Table 3. LTE and NLTE abundances from individual lines in the sample stars. This table is available in its entirety in a machine-readable form in the online version. A portion is shown here for guidance regarding its form and content.

Atom	λ (Å)	E_{exc} (eV)	$\log gf$	$\log \Gamma_6/N_H$ (rad/s·cm ³)	EW (mÅ)	$\log \epsilon$	
						LTE	NLTE
ET0381							
Na I	5889.95	0.00	0.12	-7.670	173.0	3.51	3.19
Na I	5895.92	0.00	-0.19	-7.670	143.0	3.35	3.07
Mg I	5172.68	2.71	-0.45	-7.267	197.2	5.04	5.06
Mg I	5183.60	2.72	-0.24	-7.267	204.8	4.90	4.93
Mg I	5528.41	4.35	-0.50	-7.180	59.5	4.99	5.00
Al I	3961.52	0.01	-0.34	-7.315	-1	2.72	2.82

Notes. Γ_6 corresponds to 10 000 K. The sources of the observed equivalent widths, EWs, are indicated in Table A.1.

EW = -1 means using spectral synthesis.

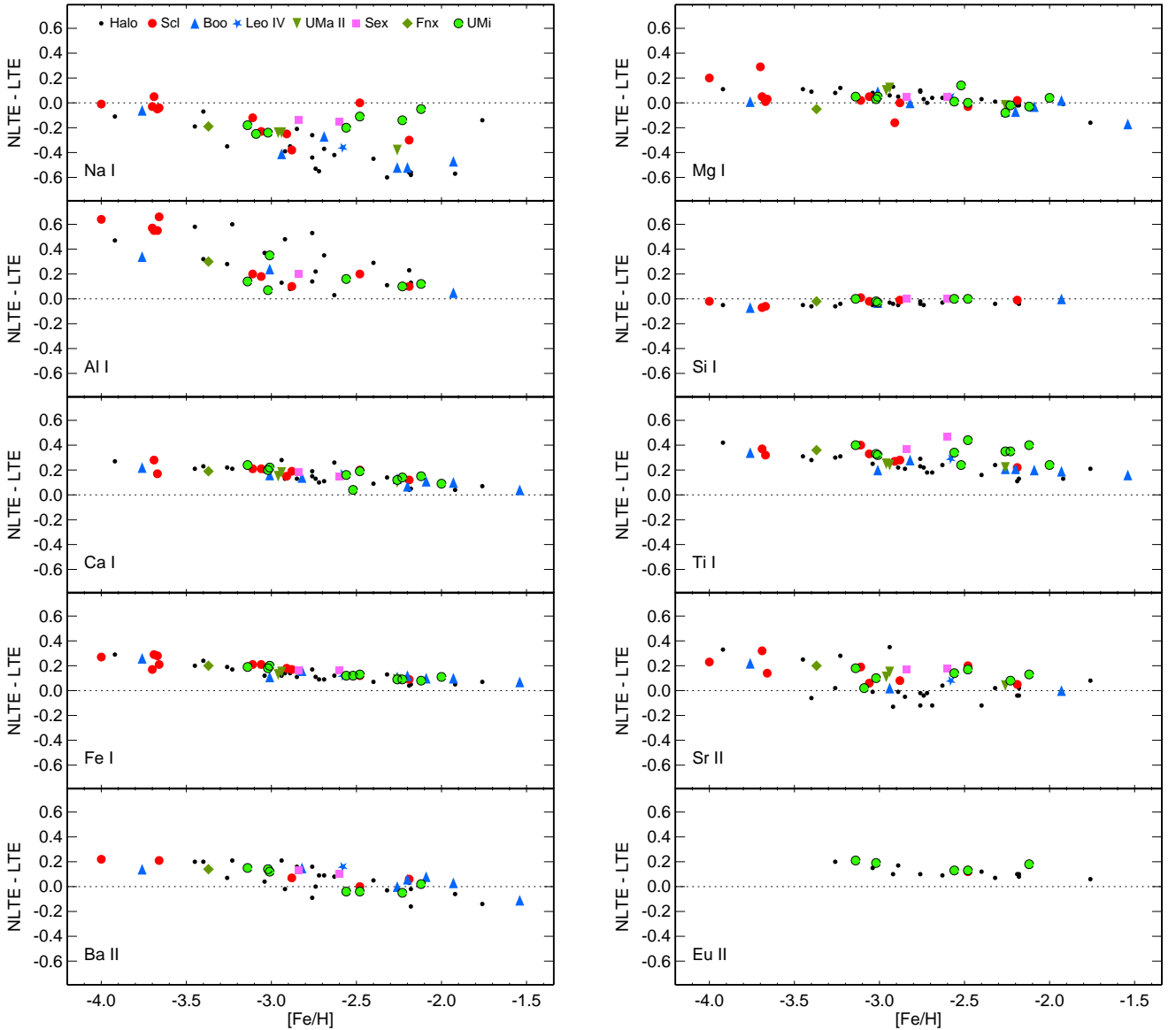


Fig. 1. Differences between the NLTE and LTE abundance of different chemical species in the Sculptor (red circles), Ursa Minor (green circles), Sextans (squares), Fornax (rhombi), Boötes I (triangles), UMa II (inverted triangles), and Leo IV (5 pointed star) dSph and the MW halo stars (small black circles).

difference between HD 8724 ($[\text{Fe}/\text{H}] = -1.76$) and HD 218857 ($[\text{Fe}/\text{H}] = -1.92$) amounts to $\Delta[\text{Mg}/\text{Fe}] = 0.24$ dex in LTE and 0.09 dex in NLTE.

4.1.4. Si I

Only small and mostly negative NLTE corrections are found for the Si I 3905 and 4102 Å lines, not exceeding 0.08 dex in absolute value. Indeed, with the accurate rate coefficients from Belyaev et al. (2014), the inelastic collisions with the neutral hydrogen atoms serve as efficient thermalising process and largely cancel the over-ionisation effect for Si I in line formation layers.

4.1.5. Na I

In contrast to the photoionisation-dominated minority species, Na I is subject to over-recombination because the photon suction process prevails over the photoionisation that is inefficient for Na I due to small cross-sections of the ground state. The over-recombination results in strengthening the Na I 5889, 5895 Å lines and negative Δ_{NLTE} . The NLTE abundance corrections vary between -0.6 and -0.01 dex. An exception is Sc1031_11 (4670/1.13/−3.69), for which the collision processes are inefficient compared to the photoionisation. Hence, the Na I lines are weaker than in LTE and $\text{NLTE-LTE} = +0.05$ dex.

Only in HD 8724 ($[\text{Fe}/\text{H}] = -1.76$), could we measure not only the Na I resonance lines, but also the subordinate lines at 5682 and 5688 Å. The NLTE treatment of Na I substantially decreases the line-to-line scatter ($\sigma_{\log \epsilon} = 0.05$ dex) compared with LTE, where $\sigma_{\log \epsilon} = 0.10$ dex. A small abundance difference of -0.14 dex between NLTE and LTE for HD 8724 is explained by including in the abundance mean the subordinate lines, for which Δ_{NLTE} is smaller, in absolute value, than that for the D₁, D₂ Na I lines, by 0.1 dex, and also by cooler T_{eff} of HD 8724 compared with that of the $[\text{Fe}/\text{H}] \simeq -2$ stars.

Similarly to Al I, Na I shows a much larger scatter of (NLTE–LTE) at fixed $[\text{Fe}/\text{H}]$ than the other species. This reflects a strong sensitivity of the departures from LTE for Na I to stellar $\log g$, T_{eff} , and the Na abundance. For example, at $[\text{Fe}/\text{H}] > -2.7$ some of the Ursa Minor (28104: 4275/0.65/−2.12), Sextans (11-04: 4380/0.57/−2.60), and Sculptor (1019417: 4280/0.5/−2.48) stars do not follow the metallicity trend in Fig. 1 that is defined by the Milky Way and Boötes I population because of the lower density of their atmospheres that weakens collisional coupling of the Na I high-excitation levels to the large continuum reservoir. For comparison, at $[\text{Fe}/\text{H}] \simeq -2.2$, HD 108317 and Boo-130 have $\log g = 2.96$ and 1.4, respectively.

4.1.6. Sr II, Ba II, and Eu II

For the majority species such as Sr II and Ba II, NLTE may either strengthen or weaken the line depending on the stellar parameter and elemental abundance, as theoretically predicted by Mashonkina et al. (1999, Ba II) and Mashonkina & Gehren (2001, Sr II). In those MW halo giants, in which the Sr abundance follows the Fe one, the Sr II 4077 and 4215 Å resonance lines are strong and the departures from LTE are small, such that Δ_{NLTE} varies between -0.15 and 0.08 dex. In the rest of the sample, the weaker the Sr II lines, the more positive NLTE correction is, up to $\Delta_{\text{NLTE}} = 0.35$ dex.

A clear metallicity trend is seen in Fig. 1 for barium, with negative NLTE–LTE for the $[\text{Fe}/\text{H}] > -2$ stars and positive one for the majority of the VMP stars. Since a change in the sign

of the NLTE abundance correction for Ba II lines depends on the stellar parameters and the element abundance itself, some of the $[\text{Fe}/\text{H}] < -2$ stars have slightly negative differences NLTE–LTE.

As discussed by Mashonkina & Gehren (2000), NLTE leads to weakened lines of Eu II and positive NLTE abundance corrections. In our cool giant sample, Δ_{NLTE} grows slowly towards lower metallicity, but never exceeds 0.2 dex.

4.2. Nickel

Nickel is observed in lines of neutral atoms that are expected to be subject to over-ionisation like other minority species, such as Al I, Fe I, etc. However, we cannot perform yet the NLTE calculations for Ni I because of the lack of a satisfactory model atom. Therefore, we assume that the ratio of abundances derived from lines of Ni I and Fe I is nearly free of the NLTE effects and use the LTE abundances in the $[\text{Ni I}/\text{Fe I}]$ versus $[\text{Fe}/\text{H}]$ diagrams. This assumption is supported by the fact that the ionisation energies of Ni I and Fe I are very similar, 7.64 eV and 7.90 eV, respectively, and these atoms have similarly complicated term structures.

4.3. Outliers

In this section, we provide comments on a few stars, which reveal peculiar abundances or any other outstanding feature.

Sculptor ET0381. This is an Fe-enhanced star, all measured chemical species being deficient relative to Fe. The LTE abundances were discussed in detail in Jablonka et al. (2015). We only find here small departures from LTE for most species. Despite an upward revision of $[\text{Fe}/\text{H}]$, by 0.25 dex, leading to slightly changed $[\text{X}/\text{Fe}]$ ratios, we confirm the conclusions of Jablonka et al. (2015). Except for $[\text{Ni}/\text{Fe}]$, this star was not used in the calculations of the average $[\text{X}/\text{Fe}]$ ratios of the Sculptor dSph.

Sc111_1_4296. In this star, the α -process elements Mg, Ca, and Ti reveal a different behaviour with respect to Fe, namely, $[\text{Mg}/\text{Fe}]$ is as low as that of ET0381, however, $[\text{Ca}/\text{Fe}]$ is higher compared with that of ET0381 and close to solar value. Titanium is enhanced relative to Fe, similarly to the remaining Sculptor dSph stars. This star was not used in the calculations of the average $[\text{Mg}/\text{Fe}]$ and $[\text{Ca}/\text{Fe}]$ ratios of the Sculptor dSph.

Sex24-72. This is a carbon enhanced star. Tafelmeyer et al. (2010) determined $[\text{C}/\text{Fe}] = 0.4$, which applying the carbon correction from Placco et al. (2014) leads to an initial $[\text{C}/\text{Fe}] \simeq 1$. It reveals also high Na abundance, with $[\text{Na}/\text{Fe}] = 0.85$ (NLTE). Combined with low abundance of the neutron-capture elements ($[\text{Sr}/\text{Fe}] = -0.43$, $[\text{Ba}/\text{Fe}] = -1.04$), Sex24-72 can be classified as a CEMP-no star.

Boo-041. We obtained higher iron abundance than that of Gilmore et al. (2013), by 0.42 dex, despite using common $T_{\text{eff}} = 4750$ K and $\log g = 1.6$. This cannot be explained by NLTE effects, because $\text{NLTE-LTE} = 0.06$ dex for Fe I. A difference of 0.25 dex in the average abundance from the Fe I lines appears already in LTE, as a consequence of lower microturbulence velocity, by 0.8 km s^{-1} , in our study. In the LTE calculations with $T_{\text{eff}} = 4750$ K, $\log g = 1.6$, and $\xi_t = 2.8 \text{ km s}^{-1}$ determined by Gilmore et al. (2013) and using 35 lines of Fe I with $E_{\text{exc}} > 1.2$ eV and $W_{\text{obs}} < 180 \text{ mÅ}$, we obtained a steep negative slope of -0.41 for the $\log \epsilon_{\text{FeI}} - \log W_{\text{obs}}/\lambda$ plot. Besides, the abundance difference $\log \epsilon_{\text{FeI}} - \log \epsilon_{\text{FeII}} = -0.22$ was uncomfortably large. We established $\xi_t = 2.0 \text{ km s}^{-1}$ by minimising the slope of the Fe I-based NLTE abundance trend with W_{obs} . This also leads to consistent NLTE abundances from the two ionisation stages

Table 4. Average NLTE abundance ratios for different stellar populations, with $\sigma_{X/Fe}$ indicated in parentheses.

[X/Fe]	Sculptor	Ursa Minor	MW halo
[Mg/Fe]	0.31 (0.19)	0.30 (0.11)	0.36 (0.13)
[Si/Fe]	0.25 (0.21)	0.03 (0.26)	0.24 (0.15)
[Ca/Fe]	0.41 (0.08)	0.24 (0.11)	0.36 (0.11)
[Ti/Fe]	0.30 (0.19)	0.32 (0.16)	0.28 (0.10)

of iron within 0.11 dex. This star reveals extremely high abundance of Ti, with $[Ti/Fe] = 0.80$, but low abundance of Ni, with $[Ni I/Fe I] = -0.52$ (LTE). Boo-041 was not used in the calculations of the average $[X/Fe]$ ratios. At $[Fe/H] = -1.54$, the Fe abundance of Boo-041 might have received the products of the type Ia supernova (SN Ia) nucleosynthesis.

4.4. Influence of uncertainties in stellar atmosphere parameters

Changes in the element abundances caused by a variation in T_{eff} , $\log g$, and ξ_t were evaluated for a part of our stellar sample in the earlier LTE analyses of Tafelmeyer et al. (2010, Table 4) and Jablonka et al. (2015, Tables 5 and 6) and the NLTE analyses of Mashonkina et al. (2010, Table 6) and Mashonkina et al. (2017, Sect. 4.2.4). When varying T_{eff} , a differential NLTE effect on the derived abundance is the largest for Al I 3961 Å, however, it does not exceed 0.03 and 0.05 dex for $\Delta T_{\text{eff}} = +100$ K around $T_{\text{eff}} = 4500$ and 5000 K, respectively. Since the sample stars have close together temperatures and surface gravities, they have also close together abundance errors due to uncertainties in atmospheric parameters. To summarise, a change of +100 K in T_{eff} produces higher abundances from lines of the minority species, such as Mg I and Al I, by 0.10-0.15 dex, and has a minor effect (≤ 0.02 dex) on the abundances from lines of the majority species, such as Ti II and Sr II. In contrast, a change of +0.1 dex in $\log g$ has a minor effect (≤ 0.01 dex) on the minority species and shifts abundances of the majority species by up to +0.05 dex. A change of +0.2 km s⁻¹ in ξ_t produces lower abundances, by 0.1 dex for the EW ≈ 120 mÅ lines and by 0.05 dex, if EW ≈ 75 mÅ.

5. Abundance trends and galaxy comparisons

Table A.1 presents the elemental LTE and NLTE abundances together with their statistical errors and the number of lines used. For consistency with our previous studies, the solar photosphere abundances are those of Anders & Grevesse (1989) at the exception of Ti and Fe, for which we consider $\log \varepsilon_{\text{Ti,met}} = 4.93$ (Lodders et al. 2009, meteoritic abundance) and $\log \varepsilon_{\text{Fe},\odot} = 7.50$ (Grevesse & Sauval 1998). The metallicities, $[Fe/H]$, as well as the abundance ratios relative to iron, $[X/Fe]$, are based on the Fe II lines. Our results are displayed in Figs. 2-9.

5.1. α -process elements

For all α -process elements, we refer to their neutral species, except for Ti for which the abundance is based on lines of Ti II. Indeed the Ti II lines are more numerous and stronger than the Ti I ones. They are also less affected by any departure from LTE. We note though that, in most of our sample stars, the abundances derived from the lines of Ti I and Ti II are consistent, as shown in Paper I.

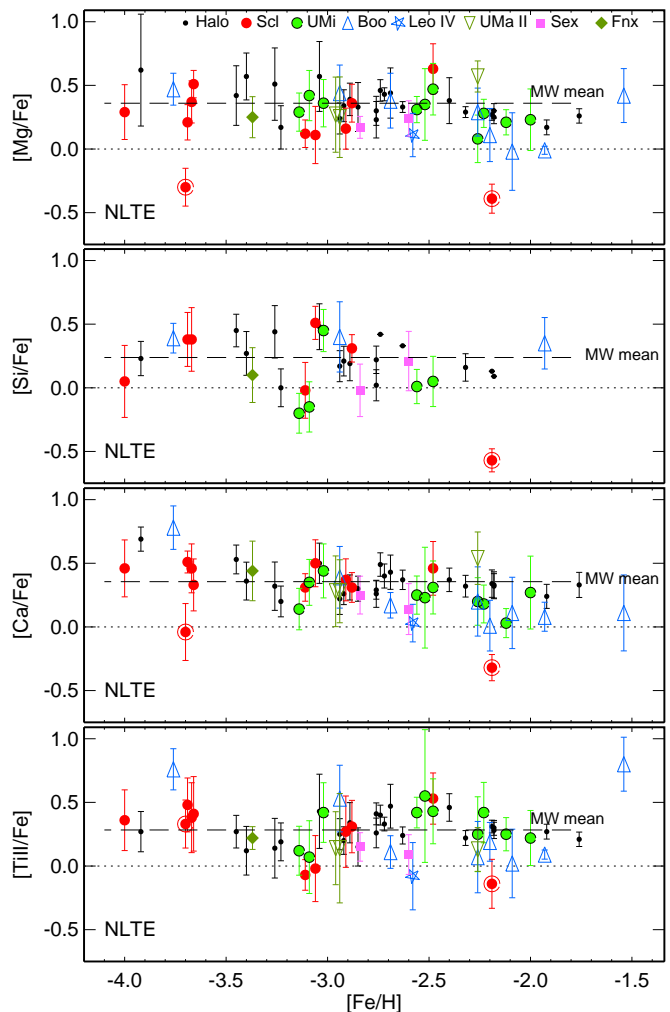


Fig. 2. Stellar element-to-iron NLTE abundance ratios for the α -process elements Mg, Si, Ca, and Ti in the Sculptor (red circles), Ursa Minor (green circles), Sextans (squares), Fornax (rhombi), Boötes I (triangles), UMa II (inverted triangles), and Leo IV (5 pointed star) dSphs and the MW halo. Two Mg-poor stars in Sculptor, 11_1_4296 and ET0381, are plotted by a red circle inside larger size open circle. The error bars were computed as $\sigma_{X/Y} = \sqrt{\sigma_X^2 + \sigma_Y^2}$. The errors of $[Fe/H]$ do not exceed 0.15 dex for most (51 of 59) stars. In each panel, the dashed line indicates the mean for the MW halo.

Before going further, it is probably worth commenting on the consequence of choosing Fe II or Fe I as a metallicity indicator on the $[X/Fe]$ versus $[Fe/H]$ diagrams. Indeed, the vast majority of the published LTE analyses are provided in function of $[Fe I/H]$. This is a consequence of the fact that the number of Fe I lines is classically much larger in the observed wavelength range. As shown in Fig. 1, the LTE treatment underestimates the iron abundance, if it is based on the Fe I lines, and NLTE–LTE (Fe I) rises towards lower metallicity. For Ca I, NLTE–LTE follows a similar trend and magnitude as Fe I, hence NLTE leaves their ratios nearly unchanged compared with LTE. Conversely, because the NLTE corrections for Mg I and Si I are minor over the $[-4, -1]$ metallicity range, $[Mg I/Fe I]$ and $[Si I/Fe I]$ are shifted downward in NLTE as compared to LTE.

Now, choosing Fe II as a metallicity indicator, $[Mg I/Fe II]$, $[Si I/Fe II]$, and $[Ti II/Fe II]$ change only a little from LTE to

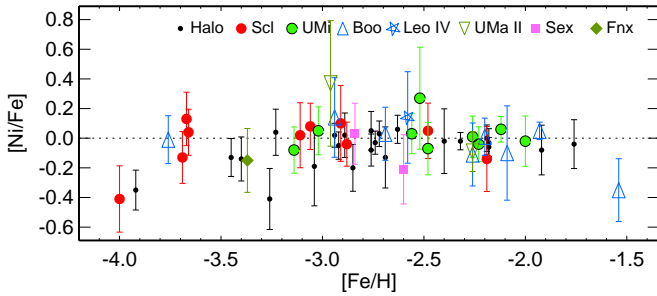


Fig. 3. Stellar $[\text{Ni I}/\text{Fe I}]$ abundance ratios. Symbols as in Fig. 2.

NLTE, while $[\text{Ca I}/\text{Fe II}]$ moves upward, because of the positive NLTE corrections for Ca I.

Because, in the NLTE treatment, we have obtained consistent Fe I- and Fe II-based abundances (Paper I), our NLTE abundance ratios $[\text{X}/\text{Fe}]$ do not depend on the choice of the metallicity tracer.

A remarkable gain of using the NLTE abundances based on a homogeneous set of atmospheric parameters is the reduction, compared to a simple compilation of the literature data (see Figs. 8 and 9 in Jablonka et al. 2015), of the spread in abundance ratios at given metallicity within each galaxy and from one to the other. This effect is particularly dramatic for Si for which the dispersion goes from a +1 dex down to ~ 0.2 dex once the Si and Fe abundances have been homogeneously revised.

Figure 2 shows that, at $[\text{Fe}/\text{H}] \leq -2.5$, all galaxies scatter around the mean of the Milky Way halo stars, $[\alpha/\text{Fe}] \approx 0.3$. Table 4 summarizes the mean elemental ratios and their dispersions for the three galaxies with a sufficient number of stars: Sculptor, Ursa Minor, and the MW halo. The outliers of Sect. 4.3 are not considered in these calculations. These numbers quantify the small star-to-star scatter (~ 0.2 dex) and show that all α -elements have similar $[\text{X}/\text{Fe}]$ means. The only apparent exception to this rule is the solar value of $[\text{Si}/\text{Fe}]$ in Ursa Minor. For the J119 star, which is the only one in this galaxy with two accessible Si I lines, $[\text{Si}/\text{Fe}] = 0.45$ ($\sigma_{\log \varepsilon} = 0.07$ dex) is close to $[\text{X}/\text{Fe}]$ for the other α -elements. The four other stars in Ursa Minor have only one Si I line at 4102 Å, which is located in a noisy region and which leads to a solar or subsolar $[\text{Si}/\text{Fe}]$ ratio. It is worth noting that our results for the MW giants are fully consistent with the NLTE abundances derived for the MW halo dwarfs by Zhao et al. (2016).

Previous LTE abundance analyses conducted at similar high spectral resolution and signal-to-noise ratios, by Tafelmeyer et al. (2010), Starkenburg et al. (2013), Jablonka et al. (2015), and Simon et al. (2015), deduced a common conclusion that the Sculptor, Sextans, and Fornax dSphs are α -enhanced in the VMP regime, at similar level to the MW halo. On the other hand, lower $[\text{Ca}/\text{Fe}]$ and $[\text{Ti}/\text{Fe}]$ than $[\text{Mg}/\text{Fe}]$ ratios were reported by Venn et al. (2004) and Cohen & Huang (2010) for the VMP stars in the Sextans and Ursa Minor dSphs. In part, these discrepancies can be caused by applying the LTE assumption. In case of using lines of Ti I and Fe I, LTE underestimates $[\text{Ti}/\text{Fe}]$ because of larger departures from LTE for the Ti I than for the Fe I lines. In contrast, $[\text{Mg I}/\text{Fe I}]$ is overestimated in the LTE analysis, as discussed in the beginning of this section. Our homogeneous NLTE analysis removes discrepancies in $[\text{X}/\text{Fe}]$ between different α -elements and between the classical dSphs and the MW halo.

We have three ultra-faint galaxies ($L \leq 10^5 L_{\odot}$) in our sample: Ursa Major II, Leo IV, and Boötes I. Interestingly, they present different features. In Ursa Major II, the three stars with very different metallicities, between $[\text{Fe}/\text{H}] \approx -3$ and -2.3 , are α -enhanced. In contrast, Leo IV and Boötes I, which are the brightest of the Local Group UFDs (McConnachie 2012), reveal a close-to-solar α/Fe ratio at $[\text{Fe}/\text{H}] \gtrsim -2.5$. Gilmore et al. (2013) had reported on a hint of a decline in $[\alpha/\text{Fe}]$ but not yet “formally significant”. The existence of a low $[\alpha/\text{Fe}]$ population is now put on a firm ground, with consistent evidence from the three elements, for which data are available, Mg, Ca, and Ti. We commented earlier that Boötes I cannot be accounted for the bulk of Boötes I population. The kinematics and morphology of Boötes I point towards a complex system (Koposov et al. 2011, Roderick et al. 2016), but as far as its chemical evolution is concerned, Boötes I, and potentially Leo IV as well, seem to simply push back the frontier, at which galaxies can reprocess the SNe Ia ejecta, with a knee at lower metallicity than their more massive counterparts, as expected from a classical chemical evolution. So far the galaxies, in which a knee in $[\alpha/\text{Fe}]$ has been found, had star formation histories of a few Gyrs long, while those of Boötes I and Leo IV are shorter (Okamoto et al. 2012). However, the nature and timescale of the type Ia supernovae are still under investigation (Kobayashi & Nomoto 2009, Nomoto et al. 2013), with the evidence for metal-poor environments having their own specific features (Taubenberger et al. 2011). Given that star formation proceeds in series of very short timescale bursts (~ 0.1 Gyr, Revaz & Jablonka 2012), it is very possible that Boötes I had enough time to form stars after its first SN Ia explosions, provided the latter occur on short timescales. The chemical evolution models by Romano et al. (2015) allow some SNe Ia to be exploded in Boötes I while it was still forming stars. An alternative possibility is that low mass SNe II have particularly contributed to the chemical evolution of the galaxy (Webster et al. 2015).

5.2. Nickel

As discussed in Sect. 4.2, we did not treat Ni in NLTE. Nevertheless, we think that the $[\text{Ni I}/\text{Fe I}]$ versus $[\text{Fe}/\text{H}]$ trend is relevant to this work. Figure 3 shows that the yields of Ni and Fe have a constant ratio and the correlation is reasonably tight. It is, in fact, tighter than with any other element produced by SNe II. Both dSph and MW halo stars are distributed around $[\text{Ni}/\text{Fe}] = 0$. We do not find in either population the high $[\text{Ni}/\text{Fe}]$ stars as in Roederer (2009). Given the large range of galaxy masses that we are sampling, this is quite remarkable. The only trend with metallicity is the increased dispersion at $[\text{Fe}/\text{H}] \leq -3$, that is, 0.15 dex instead of 0.08 dex above $[\text{Fe}/\text{H}] = -3$, which could well be explained by increasing the abundance uncertainties due to the weakening of the Ni I lines.

5.3. Odd-Z elements: Na and Al

The impact of NLTE is particularly large on the elemental ratios involving Na and Al, as a consequence of large NLTE abundance corrections for lines of Na I and Al I and their extreme sensitivity to each of the stellar parameters. The star-to-star scatter in the $[\text{Na}/\text{Fe}]$ (Fig. 4) and $[\text{Na}/\text{Mg}]$ (Fig. 5) NLTE abundance ratios is much smaller than in the LTE ones. For $[\text{Al}/\text{Fe}]$ and $[\text{Al}/\text{Mg}]$, the scatter is larger for the dSph than the MW stars, most probably, due to lower S/N ratio of the observed blue spectra and the uncertainty in analysis of Al I 3961 Å.

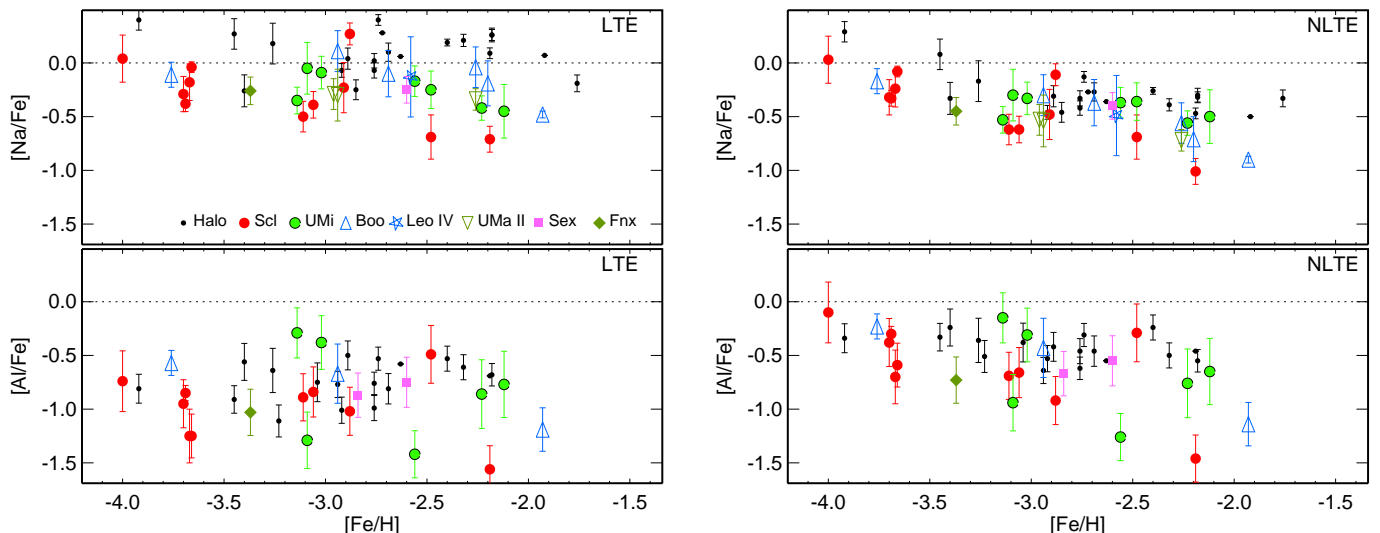


Fig. 4. Stellar $[\text{Na}/\text{Fe}]$ and $[\text{Al}/\text{Fe}]$ LTE (left column) and NLTE (right column) abundance ratios. For Sex 24-72 its LTE and NLTE ratios of $[\text{Na}/\text{Fe}] = 0.99$ and 0.85 , respectively, are not displayed. Symbols as in Fig. 1.

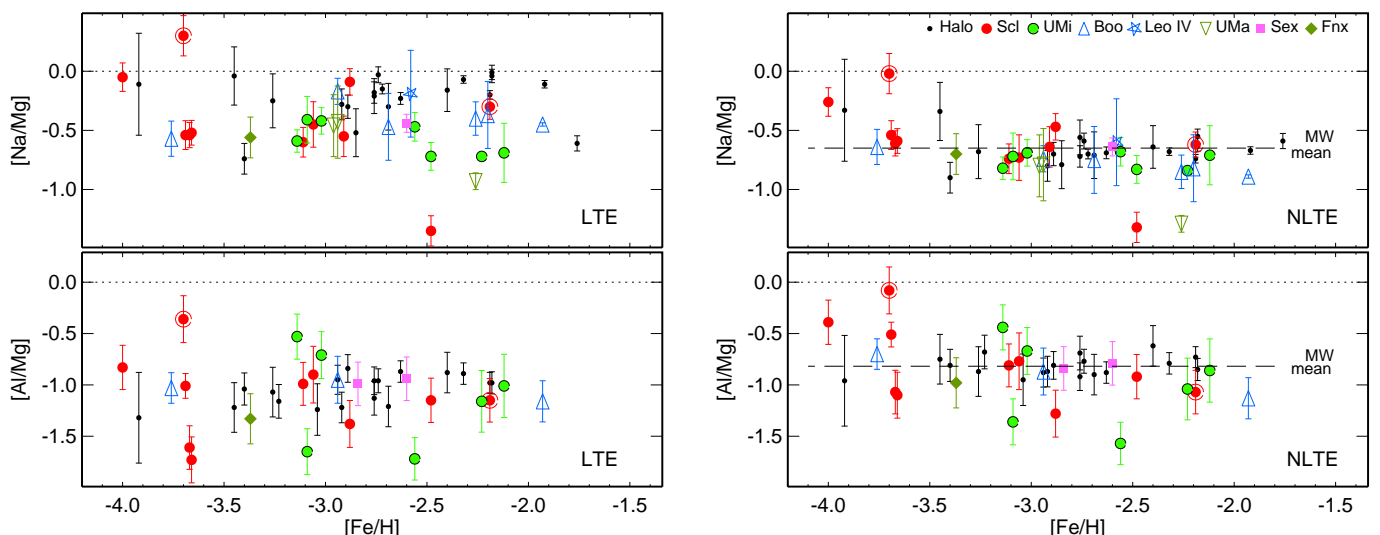


Fig. 5. Stellar $[\text{Na}/\text{Mg}]$ and $[\text{Al}/\text{Mg}]$ LTE (left column) and NLTE (right column) abundance ratios. For Sex 24-72, its NLTE ratio $[\text{Na}/\text{Mg}] = 0.68$ is not displayed. Symbols as in Fig. 2.

For $[\text{Na}/\text{Fe}]$, $[\text{Na}/\text{Mg}]$, and $[\text{Al}/\text{Mg}]$, the Milky Way and dSphs reveal indistinguishable trends with metallicity suggesting that the nucleosynthesis processes for Na and Al (carbon burning process) are identical in all systems, independent of their mass. This is in contrast to LTE, where, for the MW stars, we obtain systematically higher $[\text{Na}/\text{Fe}]$ and $[\text{Na}/\text{Mg}]$ ratios than for the dSph stars, by about 0.4 and 0.3 dex, respectively. It seems that the early production of sodium occurred in a way similar to that for the primary elements. This is confirmed by the constant $[\text{Na}/\text{Mg}] \approx -0.6$ and $[\text{Al}/\text{Mg}] \approx -0.8$ ratios in Fig. 5. The only exception to this rule is Scl11_1_4296, whose high $[\text{odd-Z}/\text{Mg}]$ ratios are only due to its depletion in Mg. The ET0381 star does not stand out in $[\text{odd-Z}/\text{Mg}]$, meaning that its Al, Na, and Mg were produced in similar relative amounts, as these elements in the other stars.

We confirm the existence of a plateau in $[\text{Na}/\text{Fe}]$ at $[\text{Fe}/\text{H}] \leq -2.0$ showed in Andrievsky et al. (2007). These authors re-

ported a mean value of $[\text{Na}/\text{Fe}] = -0.2$, while we find $[\text{Na}/\text{Fe}] = -0.4$. The difference between the two studies arises, probably, from the fact that Andrievsky et al. (2007) used the iron LTE abundances and, hence, underestimated $[\text{Fe}/\text{H}]$ values. Just as us here, Andrievsky et al. (2007) showed a hint of a rise in $[\text{Na}/\text{Fe}]$ below $[\text{Fe}/\text{H}] = -3.5$. As discussed in Paper I, the NLTE ionisation balance between Fe I and Fe II is not fully satisfied for the Sculptor stars in this region. Hence we might actually underestimate $[\text{Fe}/\text{H}]$ by a bit by referring to Fe II. The Milky Way star at $[\text{Fe}/\text{H}] = -3.92$, HE1357-0123, with more than 0.2 dex difference between its Fe I- and Fe II-based abundances, also follows the $[\text{Na}/\text{Fe}]$ rising trend, calling for further investigation.

Going from LTE to NLTE changes dramatically the picture of early enrichment of the MW and the dSphs in Na and Al. In NLTE, sodium is found to be slightly overabundant relative to aluminum, with the mean of $[\text{Na}/\text{Al}] \sim 0.2$ dex, while substantially larger ratio of $[\text{Na}/\text{Al}] \sim 0.8$ is obtained in LTE.

For clarity, we did not include a carbon-enhanced star Sex24-72 in the $[\text{Na}/\text{Fe}]$ panel of Fig. 4. This is one of the very rare CEMP-no stars found in a classical dSph (Skúladóttir et al. 2015). Tafelmeyer et al. (2010) have measured $^{12}\text{C}/^{13}\text{C} = 6$ in this star, a clear indication of internal mixing (see, for example, Spite et al. 2006). We determine $[\text{Na}/\text{Fe}] = 0.85$, $[\text{Na}/\text{Mg}] = 0.68$, and $[\text{Na}/\text{Al}] = 1.52$, hence, a clear overabundance of sodium. Unlike the mixed stars in Spite et al. (2006), the $[\text{Al}/\text{Mg}]$ ratio of Sex24-72 does not stand out from our other sample stars, and this star is not particularly Mg poor. Therefore, the abundance pattern of Sex24-72 was not affected by the Mg-Al cycle. We conclude that the Na overabundance of Sex24-72 is a consequence of the extra-mixing between the atmosphere and the H-burning shell, which was deep enough to bring the products of the Ne-Na cycle to the surface.

5.4. Neutron-capture elements: Sr and Ba

Despite many theoretical and observational studies of the neutron-capture elements in the long-lived stars in our Galaxy, there are not yet clear answers to the following questions: what is (are) the astrophysical site(s) of the rapid (r) process of neutron-capture nuclear reactions, what types of nuclear reactions produced the light trans-iron elements, Sr-Zr, in the early Universe and at what astrophysical site(s), and did the light and heavy (beyond Ba) elements originate from a common astrophysical site.

It is beyond the scope of this work to provide any definitive answers. However, the homogeneity of our abundance analysis and our compilation of galaxies with very different evolutionary paths do provide a few clear evidence that can constrain future models.

The left panels of Fig. 6 present the variation of Ba and Sr relative to Fe as a function of metallicity in a classical manner. At first glance both $[\text{Sr}/\text{Fe}]$ and $[\text{Ba}/\text{Fe}]$ present a very large scatter at any given $[\text{Fe}/\text{H}]$. A closer look though reveals different behaviours, which depend on the metallicity range and on the galaxy: i) $[\text{Fe}/\text{H}] \approx -2.8$ is a metallicity threshold below and above which the dispersion in abundance ratio changes and ii) massive and fainter galaxies do not follow the same trend.

We first concentrate on our MW halo sample. In both LTE and NLTE abundance analyses, $[\text{Sr}/\text{Fe}]$ and $[\text{Ba}/\text{Fe}]$ have large dispersion below $[\text{Fe}/\text{H}] \approx -2.8$, as also shown by Andrievsky et al. (2009, 2011) and Hansen et al. (2013). Above this metallicity, $[\text{Sr}/\text{Fe}]$ becomes steadily solar. As to $[\text{Ba}/\text{Fe}]$, the rise to the solar value comes at slightly higher metallicity, $[\text{Fe}/\text{H}] \approx -2.5$. Although largely diminished, the dispersion is larger than for $[\text{Sr}/\text{Fe}]$.

Europium abundances are available for 11 stars of our MW sample and, in particular, for all stars but HD 218857 (because its spectrum does not extend blue enough) at $[\text{Fe}/\text{H}] > -2.5$. Figure 7 shows that all these stars have $[\text{Eu}/\text{Ba}] \geq 0.28$, a value much closer to the r-process $[\text{Eu}/\text{Ba}]_r = 0.80$ (based on the solar r-residuals, Bisterzo et al. 2014) than the s-process $[\text{Eu}/\text{Ba}]_s = -1.15$ ratio. This reflects the fact that if there is a contribution of the s-process to the Ba abundances, it is only a minor one. We stress that we discard the most metal-rich star of our sample, HD 8724, with $[\text{Fe}/\text{H}] = -1.76$ and $[\text{Eu}/\text{Ba}] = 0.21$, from any discussion on very metal-poor stars.

Would Ba and Sr be produced by the same nucleosynthesis source, this should result in a fairly flat (within observational error bars) $[\text{Sr}/\text{Ba}]$ ratio versus $[\text{Ba}/\text{H}]$. This is clearly not the case in Fig. 8. Our MW halo sample is separated into two groups. The first one that includes eight of 20 stars has indeed similar $[\text{Sr}/\text{Ba}] \sim -0.5$ on the entire range of Ba abun-

dances. Although astrophysical site(s) of the r-process is (are) not identified yet (Wanajo et al. 2014, Nishimura et al. 2017), the strongly r-process enhanced ($[\text{Eu}/\text{Fe}] > 1$, $[\text{Eu}/\text{Ba}] > 0$) stars referred to as r-II stars (Christlieb et al. 2004) provide an observational evidence for the r-process to yield a subsolar Sr/Ba ratio. We estimate the empirical r-process ratio, $[\text{Sr}/\text{Ba}]_r = -0.38$, using the six halo r-II stars: CS 22892-052 (Snedden et al. 2003), HE1219-0312 (Hayek et al. 2009), SDSS J2357-0052 (Aoki et al. 2010), HE2327-5642 (Mashonkina et al. 2010), CS 31082-001 (Siqueira Mello et al. 2013), and CS 29497-004 (Hill et al. 2016). It is worth noting that a sample of 253 metal-poor halo stars in Barklem et al. (2005) includes eight r-II stars and they all have the lowest and similar Sr/Ba, with the mean $[\text{Sr}/\text{Ba}]_{r\text{-II}} = -0.44 \pm 0.08$ that is very close to our estimate of $[\text{Sr}/\text{Ba}]_r$. The question is whether the observed subsolar Sr/Ba ratio itself can be considered as a signature of the r-process origin of Sr.

The second MW group seems to be aligned on a well-defined downward trend of $[\text{Sr}/\text{Ba}]$ with $[\text{Ba}/\text{H}]$. Similar tight anti-correlation of $[\text{Sr}/\text{Ba}]$ with $[\text{Ba}/\text{Fe}]$ and $[\text{Ba}/\text{H}]$ was reported by Honda et al. (2004) and François et al. (2007). In line with Barklem et al. (2005), we obtained that an enhancement of Sr relative to Ba correlates with the stellar Eu abundance (Fig. 7): no star with supersolar Sr/Ba ratio is enhanced in Eu, while the stars with subsolar Sr/Ba ratios have $[\text{Eu}/\text{Fe}] \geq 0.36$.

In order to explain an excess of Sr production relative to the classical r-process, various ideas and models were proposed: i) the weak s-process during the hydrostatic core He-burning phase of massive stars (Raiteri et al. 1991), ii) charged particle reactions in core-collapse supernovae (Woosley & Hoffman 1992), iii) nucleosynthesis from progenitor stars that lived and died prior to the formation of the first "main" r-process stars (Truran et al. 2002); iv) non-standard s-process in low metallicity massive rotating stars (Pignatari et al. 2008); v) explosive nucleosynthesis in a high energy SN (or "hypernova") (Izutani et al. 2009); vi) rapid charged-particle reactions in the high-entropy winds at low entropies (Farouqi et al. 2010); vii) neutron star mergers (Tsujimoto & Shigeyama 2014, Wanajo et al. 2014); viii) the weak r-process (referred also to as alpha-process) taking place in neutrino-driven winds (Bliss et al. 2017), and ix) the intermediate r-process in core-collapse supernovae driven by the magneto-rotational instability (Nishimura et al. 2017). However, the source(s) is (are) not identified yet.

The confrontation of galaxies with very different star formation histories and chemical evolution paths provides new abundance trends and should help to constrain the nucleosynthesis origins of the neutron-capture elements.

We find differences in the abundance trends between the classical dSphs (Sculptor, Ursa Minor, Fornax, Sextans) and the UFDs (Boötes I, UMa II) and, for the classical dSphs, differences between the elemental ratios involving Sr and Ba. The main observational results can be summarised as follows.

Keeping the same distinctive two regions below and above $[\text{Fe}/\text{H}] \approx -2.8$, -2.5 for Sr and Ba, respectively, Fig. 6 shows that the classical dSph and the MW halo stars behave identically in the low-metallicity regions, with large dispersions in $[\text{Sr}/\text{Fe}]$ or $[\text{Ba}/\text{Fe}]$ in both cases.

In the two UFDs, Boötes I and UMa II, all the stars are depleted in Sr and Ba relative to Fe, with very similar ratios of $[\text{Sr}/\text{Fe}] \approx -1.1$ and $[\text{Ba}/\text{Fe}] \approx -0.75$ on the entire range of metallicity (Fig. 6). Their Ba/Fe ratio is close to the Ba/Fe floor of the MW halo, while Sr/Fe is higher than that for the most Sr-poor stars in the MW, by more than 0.5 dex. The Sr/Fe ratio of the

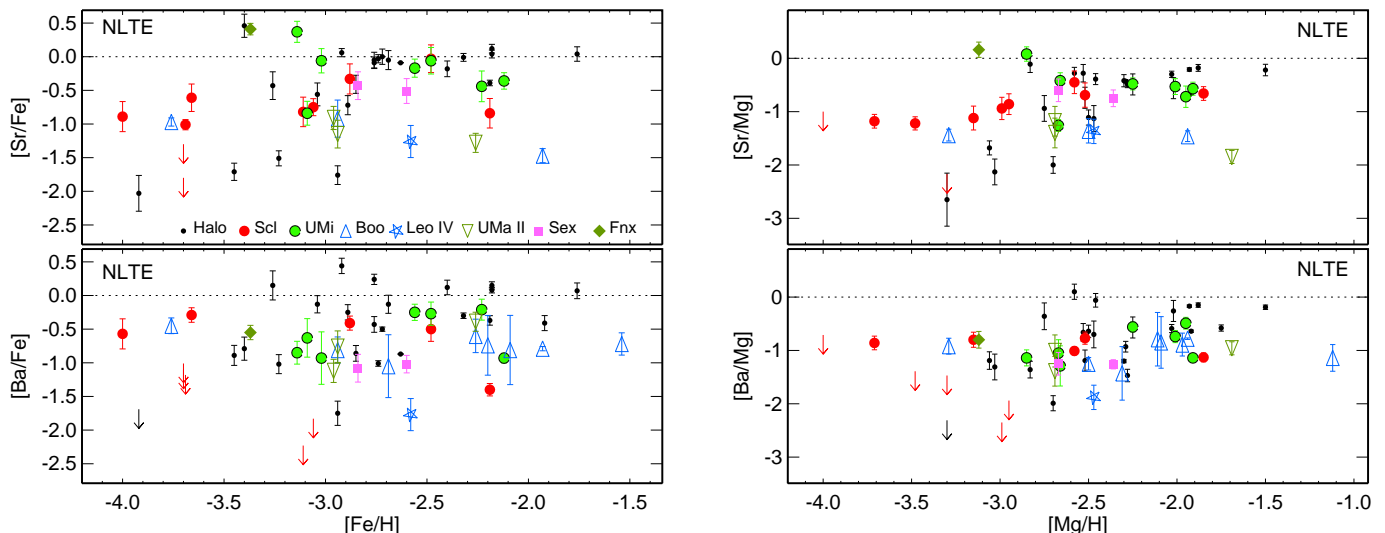


Fig. 6. Left column: $[\text{Sr}/\text{Fe}]$ and $[\text{Ba}/\text{Fe}]$ NLTE abundance ratios as a function of metallicity for our sample stars. Right column: $[\text{Sr}/\text{Mg}]$ and $[\text{Ba}/\text{Mg}]$ NLTE abundance ratios as a function of Mg abundance. Symbols and colours are as in Fig. 2. Upper limits in the Ba and Sr abundances are indicated with arrows.

only star available in Leo IV-S1 does not stand out of the corresponding ratios in Boötes I and UMa II, but Ba/Fe is lower, by one order of magnitude, although remains at the level of Ba/Fe for the MW most Ba-poor stars. Low $[\text{Ba}/\text{Fe}]$ ratios had been reported by Frebel et al. (2010) and Kirby & Cohen (2012) based on their LTE analyses. The improvement here is that homogeneity of the analysis allows to accurately compare the levels of the stellar abundance ratios.

In order to put all galaxies on the same footing and, in particular, to remove any potential pollution of the iron abundances by the ejecta of SNeIa that would affect some galaxies at $[\text{Fe}/\text{H}] \geq -2.8$ but not the others, we now consider the evolution of Ba and Sr relatively to Mg, as shown in the right panels of Fig. 6. The same conclusions, as drawn below, would be reached, should one consider any other α -element.

The dichotomy seen previously remains. Large scatter of data below $[\text{Mg}/\text{H}] \approx -2.6$ in the massive galaxies confirms that their early enrichment in Ba and Sr is produced in a variety of conditions, sufficiently rare and with varying yields for the interstellar medium to remain inhomogeneous. A more ordered behaviour of Sr/Mg and Ba/Mg is observed above $[\text{Mg}/\text{H}] \approx -2.6$. Strontium and barium present different features though.

For Sr/Mg, there are two clear sequences at $[\text{Mg}/\text{H}] \gtrsim -2.6$, one scattering around $[\text{Mg}/\text{H}] \approx -0.37$, which gathers the MW halo stars and the most massive (classical) dwarfs, such as Sextans, Ursa Minor and Sculptor, while the UFDs Leo IV, UMa II, and Boötes I keep remarkably consistent and low abundance ratios, at the level of $[\text{Sr}/\text{Mg}] \approx -1.3$. This means that while the stellar population of massive dSphs as well as the MW halo can rise their abundance of Sr relatively to Mg, the UFDs cannot and miss this additional Sr production channel.

As to Ba, again similar ratios, at the level of $[\text{Ba}/\text{Mg}] \sim -1$, are found in the UFDs Boötes I and UMa II on the entire Mg abundance range. In the classical dSphs, the scatter of Ba/Mg is reduced above $[\text{Mg}/\text{H}] \approx -2.4$, but much less than for Sr/Mg, and one does not witness any particular differential behaviour between the classical and faint dwarfs. While the dSph stars populate $[\text{Ba}/\text{Mg}]$ regions where one finds the MW stars as well, it

is fair to say that they do not reach as high ratios as our MW sample stars.

Previous LTE observational investigations, comparing dwarf spheroidal galaxies with the Milky Way halo population, have shown evidence for more than one channel of production of the neutron-capture elements lighter than Ba (Cohen & Huang 2010, Frebel et al. 2010, Tafelmeyer et al. 2010, Kirby & Cohen 2012, Jablonka et al. 2015, Roederer 2017). However, at this stage the question of the different production origins is still wide open. Our goal in the following is to provide concrete evidence and constraints that can be further used to improve theoretical models.

Since neither Fe nor Mg is a good tracer for the heavy or light neutron-capture elements, we inspect the Sr/Ba ratio as a function of $[\text{Ba}/\text{H}]$ (Fig. 8).

For the UFDs, the statistics of Sr/Ba is even poorer than that for the Sr abundances. Five of our seven stars in the UFDs with such measurements have subsolar $[\text{Sr}/\text{Ba}]$, -0.11 down to -0.89 , suggesting a common origin of the neutron-capture elements in the Boötes I and UMa II stars in the classical main r-process. The analysis of the r-process-rich galaxy Reticulum II has provided evidence for a variety of evolution among UFDs and a reference to the r-process enhanced stars in these systems, which have similar $[\text{Sr}/\text{Ba}]$ ratios of -0.21 to -1.17 (Ji et al. 2016, Roederer et al. 2016).

The classical dSphs follow the trends defined by the MW halo stars, either at subsolar $[\text{Sr}/\text{Ba}]$ or along the upward $[\text{Sr}/\text{Ba}]$ trend with decreasing $[\text{Ba}/\text{H}]$. In the Sculptor dSph, the upward trend extends, probably, to $[\text{Ba}/\text{H}] \sim -5$. Indeed, we have the two stars, Scl002_06 and Scl074_02, where the Ba II 4934 Å resonance line could not be measured resulting in $[\text{Sr}/\text{Ba}] > 1.1$, while their $[\text{Ba}/\text{H}] \lesssim -5$. For our MW sample, the statistics of Sr/Ba measurements at $[\text{Ba}/\text{H}] < -4$ is poor, however, the upward $[\text{Sr}/\text{Ba}]$ trend extending down to $[\text{Ba}/\text{H}] \approx -5$ was reported by Honda et al. (2004).

The well delineated branch at $[\text{Sr}/\text{Ba}] \geq 0$ is built from stars of increasing Ba and stable Sr abundances. This is seen in Fig. 6 (right column) and even more clearly in Fig. 9. For these stars, Sr scales perfectly with Mg over the range of $[\text{Ba}/\text{H}]$ considered

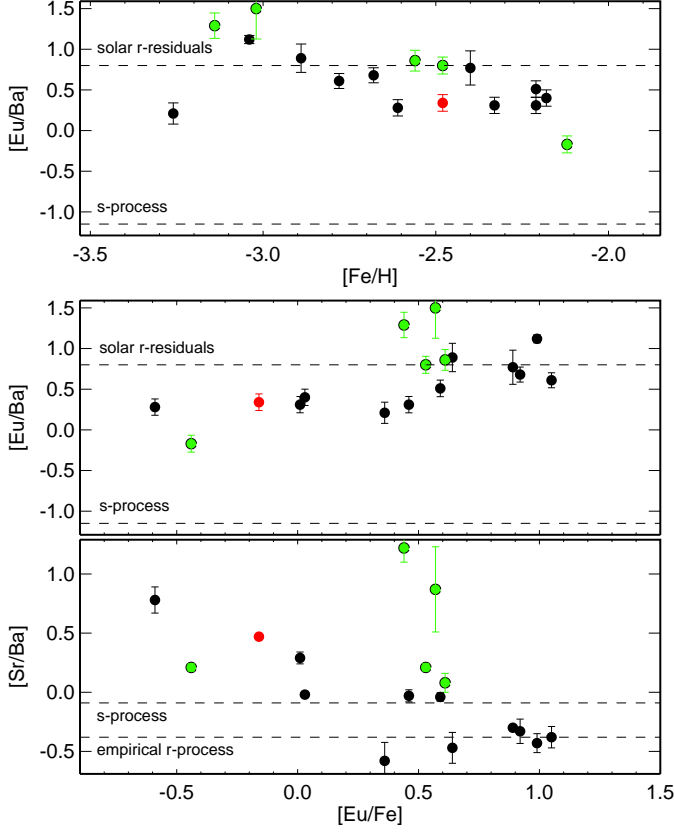


Fig. 7. Stellar [Eu/Ba] (top and middle panels) and [Sr/Ba] (bottom panel) NLTE abundance ratios in the MW halo (black circles) and the Sculptor (red circle) and Ursa Minor (green circles) dSphs. The dashed lines indicate the r- and s-process ratios $[\text{Eu}/\text{Ba}]_r = 0.80$, $[\text{Eu}/\text{Ba}]_s = -1.15$, and $[\text{Sr}/\text{Ba}]_s = -0.09$ according to Bisterzo et al. (2014) and our empirical estimate of $[\text{Sr}/\text{Ba}]_r = -0.38$.

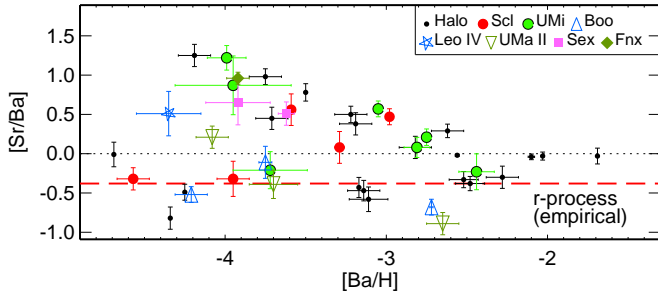


Fig. 8. The [Sr/Ba] NLTE abundance ratios as a function of Ba abundance. The dashed line indicates the mean [Sr/Ba] ratio of the six r-II stars (see text). Symbols and colours are as in Fig. 6.

for the branch, implying that the second producer of strontium in the $-4 \lesssim [\text{Ba}/\text{H}] \lesssim -2.5$ regime of the MW halo and the classical dSphs is independent of the production of barium and connected with massive stars. In the meantime, the lower panel is very quickly independent of these.

Different mass galaxies: the MW halo, the classical dSphs in Sculptor, Sextans, Fornax, and Ursa Minor, and the Boötes I and UMa II UFDs reveal similar [Ba/Mg] ratios in the $-4.3 \lesssim [\text{Ba}/\text{H}] \lesssim -3.5$ range (Fig. 9), suggesting similar efficiency of Ba production via massive stars. At the higher Ba abundances,

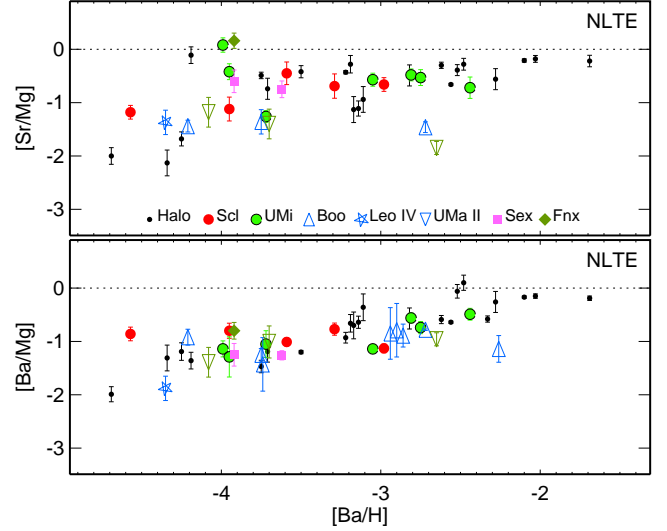


Fig. 9. The [Sr/Mg] and [Ba/Mg] abundance ratios versus [Ba/H]. Symbols as in Fig. 6.

Ba/Mg grows in the massive galaxies, while remains at low level in the UFDs.

6. Conclusions

The aim of this paper is to provide the community with a robust framework for galaxy chemical evolution studies. For that purpose, we have assembled a sample of galaxies with very different evolutionary paths, benefiting from high-resolution spectroscopy ($R \geq 25\,000$) coming from a variety of sources. In Paper I we presented a homogeneous set of accurate atmospheric parameters. In this study, we determined the NLTE abundances of ten chemical species in the giant stars covering the $-4 < [\text{Fe}/\text{H}] < -1.7$ metallicity range and belonging to the Milky Way halo (23 stars), as well as the Sculptor, Ursa Minor, Sextans, and Fornax classical dSphs and the Boötes I, UMa II, and Leo IV UFDs (36 stars). This is the first time that *all* abundances are derived under NLTE.

For each star, abundances of Na, Mg, Al, Si, Ca, Ti, Fe, Ni, Sr, and Ba were obtained, provided the corresponding lines could be measured. The NLTE effects on the derived abundances are found to be different in magnitude and sign, depending on the chemical species and the atmospheric parameters.

The first major impact of a homogeneous set of atmospheric parameters combined with a NLTE treatment is a substantial reduction of the spread in abundance ratios at given metallicity, compared to a simple compilation of the literature data. It influences the abundance trends as follows.

- Any discrepancy in the level of the $[\alpha/\text{Fe}]$ plateau between different α -elements: Mg, Ca, and Ti is now removed. It is valid for all galaxies and particularly visible for the most populated ones in our sample, Sculptor, Ursa Minor, and the MW halo.
- In the $[\alpha/\text{Fe}]$ versus metallicity diagrams, all classical dSphs: Sculptor, Ursa Minor, Sextans, and Fornax scatter around the mean of the Milky Way halo stars, $[\alpha/\text{Fe}] \approx 0.3$, suggesting enrichment of these galaxies by the massive stars, in numbers following classical IMF. It is worth stressing that our results for the MW giants are fully consistent with the NLTE abundances derived for the MW halo dwarfs by Zhao et al. (2016).

- The most dramatic effect of NLTE is found for the Na/Al abundance ratios. The LTE analysis suggests substantial overabundance of sodium relative to aluminum in all types of galaxies, at the level of $[\text{Na}/\text{Al}] \sim 0.8$, while $[\text{Na}/\text{Al}]$ is reduced down to ~ 0.2 in NLTE.
- For $[\text{Na}/\text{Fe}]$, $[\text{Na}/\text{Mg}]$, and $[\text{Al}/\text{Mg}]$, the Milky Way and dSphs reveal indistinguishable trends with metallicity suggesting that the processes of Na and Al synthesis (carbon burning process) are identical in all systems, independent of their mass.
- The relation between Ni and Fe is extremely tight, much tighter than with any other element produced by SNeII.

The abundance trends deliver important clues on the galaxy star formation histories. We could firmly assess the impact of SNeIa ejecta on the chemical evolution of some of the faintest dwarfs known.

- The Boötes I UFD reveals a decline in α/Fe and possesses a low $[\alpha/\text{Fe}]$ population, with consistent evidence from the three elements for which data are available, Mg, Ca, and Ti. This can be a signature of the SNeIa contribution to iron and a duration of about 1 Gyr for star formation in this galaxy.
- The low $[\alpha/\text{Fe}]$ value of the S1 star in the Leo IV UFD suggests that this galaxy had a long enough star formation history to be polluted by SNeIa ejecta.
- In contrast, Ursa Major II ($M_V = -4.2$), which is the faintest of our three UFDs (McConnachie 2012) and has three stars that cover the $-3 < [\text{Fe}/\text{H}] < -2.3$ metallicity range, falls exactly on the $[\text{Mg}/\text{Fe}]$ and $[\text{Ca}/\text{Fe}]$ plateau formed by the MW halo stars, indicating the dominance of SNeII in its chemical evolution and a short formation timescale.

We bring in constraints on nucleosynthesis sites, particularly for the neutron-capture elements, and on the mixing of the SN ejecta in the galaxy interstellar medium and provide further evidence that the mass of a galaxy is an important driver of its chemical evolution.

- Inhomogeneous mixing and/or stochastic effects from small numbers of SNe II is robustly documented in the Sculptor dSph. One star, ET0381, is strongly deficient in all elements except for the Fe-group, possibly missing the ejecta of the most massive Type II supernovae (Jablonka et al. 2015). The star 11_1_4296 is Mg- and Ca-poor. The two $[\text{Fe}/\text{H}] \simeq -3$ stars, 002_06 and 074_02, show no signature of the Ba II 4934 Å resonance line in their spectra, suggesting substantially lower Ba abundance, by more than 1 dex, compared with that of the star 03_059 which has a similar metallicity. Neither Ba, nor Sr can be measured in the two $[\text{Fe}/\text{H}] \simeq -3.7$ stars, 11_1_4296 and S1020549, while the Sr II and Ba II lines are reliably detected in two other stars with almost the same metallicity and even in the EMP star 07-50.
- The classical dSphs behave like the MW halo with respect to $[\text{Sr}/\text{Fe}]$: large dispersion below $[\text{Fe}/\text{H}] \sim -3$, but close-to-solar Sr/Fe ratio above this metallicity. Magnesium seems to be a better tracer of the Sr evolution than iron. In the investigated metallicity range, none of the classical dSphs reaches a solar Ba/Fe nor Ba/Mg ratio.
- Magnesium seems to be a better tracer of strontium than iron. Even though their $[\text{Ba}/\text{Mg}]$ ($[\text{Ba}/\text{Fe}]$) increases with time ($[\text{Mg}/\text{H}]$ or $[\text{Fe}/\text{H}]$), none of the classical dSphs reaches a solar Ba/Mg (Ba/Fe) ratio.

- The massive dSphs follow the Sr/Ba trends defined by the MW halo stars, either at subsolar value or along the declining $[\text{Sr}/\text{Ba}]$ trend with increasing $[\text{Ba}/\text{H}]$. This suggests two different nucleosynthesis channels for Sr.
- We show evidence for that the production of Sr is independent of Ba in the $-4 \lesssim [\text{Ba}/\text{H}] \lesssim -2.5$ regime of the massive galaxies. Nearly constant $[\text{Sr}/\text{Mg}]$ ratios suggest a strong link to massive stars, unlike Ba.
- The UFDs are depleted in Sr and Ba relative to Fe and Mg, with very similar ratios of $[\text{Sr}/\text{Mg}] \simeq -1.3$ and $[\text{Ba}/\text{Mg}] \simeq -1$ on the entire range of metallicity (and Mg abundance) for Boötes I and UMa II. The only star available in Leo IV does not stand out with respect to $[\text{Sr}/\text{Mg}]$, while its lower $[\text{Ba}/\text{Mg}]$ ratio compared with that for the other two UFDs is probably related to the early dispersed mode of Ba production. Subsolar Sr/Ba ratios of the stars in Boötes I and UMa II may indicate a common origin of Sr and Ba in the classical main r-process, though the statistics of Sr/Ba measurements is poor. The fact that the faint galaxies miss the second channel of Sr production could be explained by an undersampling of the IMF, possibly at its high-tail.

This study is the first step to our goal of further NLTE high-resolution studies of dSphs. We plan to increase the number and mass range of the galaxies explored, and to extend the observed metallicity range of their populations.

Acknowledgements. We thank Judith G. Cohen, Rana Ezzeddine, Anna Frebel, and Joshua D. Simon for providing stellar spectra, David Yong for double checking the observed equivalent widths of the Ba II lines in the Boötes I stars. The authors are indebted to the International Space Science Institute (ISSI), Bern, Switzerland, for supporting and funding the international team "The Formation and Evolution of the Galactic Halo". L.M., Y.P., and T.S. acknowledge financial support from the grant on Leading Scientific Schools 9951.2016.2. We made use of the MARCS, SIMBAD, and VALD databases.

References

- Alexeeva, S., Pakhomov, Y., & Mashonkina, L. 2014, *Astronomy Letters*, 40, 406
- Anders, E. & Grevesse, N. 1989, *Geochim. Cosmochim. Acta*, 53, 197
- Andrievsky, S. M., Spite, F., Korotin, S. A., et al. 2011, *A&A*, 530, A105
- Andrievsky, S. M., Spite, M., Korotin, S. A., et al. 2010, *A&A*, 509, A88
- Andrievsky, S. M., Spite, M., Korotin, S. A., et al. 2007, *A&A*, 464, 1081
- Andrievsky, S. M., Spite, M., Korotin, S. A., et al. 2008, *A&A*, 481, 481
- Andrievsky, S. M., Spite, M., Korotin, S. A., et al. 2009, *A&A*, 494, 1083
- Aoki, W., Beers, T. C., Honda, S., & Carollo, D. 2010, *ApJ*, 723, L201
- Arlandini, C., Käppeler, F., Wisshak, K., et al. 1999, *ApJ*, 525, 886
- Asplund, M. 2005, *ARA&A*, 43, 481
- Barklem, P. S., Belyaev, A. K., Dickinson, A. S., & Gad ea, F. X. 2010, *A&A*, 519, A20
- Barklem, P. S., Belyaev, A. K., Spielfiedel, A., Guitou, M., & Feautrier, N. 2012, *A&A*, 541, A80
- Barklem, P. S., Christlieb, N., Beers, T. C., et al. 2005, *A&A*, 439, 129
- Barklem, P. S., Piskunov, N., & O'Mara, B. J. 2000, *A&AS*, 142, 467
- Baumueler, D., Butler, K., & Gehren, T. 1998, *A&A*, 338, 637
- Baumueler, D. & Gehren, T. 1996, *A&A*, 307, 961
- Baumueler, D. & Gehren, T. 1997, *A&A*, 325, 1088
- Bautista, M. A., Gull, T. R., Ishibashi, K., Hartman, H., & Davidson, K. 2002, *MNRAS*, 331, 875
- Becker, W. & Werth, G. 1983, *Zeitschrift fur Physik A Hadrons and Nuclei*, 311, 41
- Belyaev, A. K. 2013, *A&A*, 560, A60
- Belyaev, A. K., Yakovleva, S. A., & Barklem, P. S. 2014, *A&A*, 572, A103
- Belyaev, A. K., Yakovleva, S. A., Guitou, M., et al. 2016, *A&A*, 587, A114
- Belyakova, E. V. & Mashonkina, L. I. 1997, *Astronomy Reports*, 41, 530
- Bergemann, M. 2011, *MNRAS*, 413, 2184
- Bergemann, M., Hansen, C. J., Bautista, M., & Ruchti, G. 2012, *A&A*, 546, A90
- Bisterzo, S., Travaglio, C., Gallino, R., Wiescher, M., & Käppeler, F. 2014, *ApJ*, 787, 10
- Blatt, R. & Werth, G. 1982, *Phys. Rev. A*, 25, 1476

- Bliss, J., Arcones, A., Montes, F., & Pereira, J. 2017, *Journal of Physics G Nuclear Physics*, 44, 054003
- Borghs, G., de Bisschop, P., van Hove, M., & Silverans, R. E. 1983, *Hyperfine Interactions*, 15, 177
- Brix, P. & Kopfermann, H. 1952, *Landolt-Börnstein*, I/5 (Springer, Berlin)
- Butler, K. & Giddings, J. 1985, *Newsletter on the analysis of astronomical spectra*, No. 9, University of London
- Christlieb, N., Beers, T. C., Barklem, P. S., et al. 2004, *A&A*, 428, 1027
- Cohen, J. G., Christlieb, N., Thompson, I., et al. 2013, *ApJ*, 778, 56
- Cohen, J. G. & Huang, W. 2010, *ApJ*, 719, 931
- Drawin, H.-W. 1968, *Zeitschrift für Physik*, 211, 404
- Farouqi, K., Kratz, K.-L., Pfeiffer, B., et al. 2010, *ApJ*, 712, 1359
- François, P., Depagne, E., Hill, V., et al. 2007, *A&A*, 476, 935
- Frebel, A., Norris, J. E., Gilmore, G., & Wyse, R. F. G. 2016, *ApJ*, 826, 110
- Frebel, A., Simon, J. D., Geha, M., & Willman, B. 2010, *ApJ*, 708, 560
- Gehren, T., Liang, Y. C., Shi, J. R., Zhang, H. W., & Zhao, G. 2004, *A&A*, 413, 1045
- Gilmore, G., Norris, J. E., Monaco, L., et al. 2013, *ApJ*, 763, 61
- Grevesse, N. & Sauval, A. J. 1998, *Space Sci. Rev.*, 85, 161
- Grevesse, N. & Sauval, A. J. 1999, *A&A*, 347, 348
- Gustafsson, B., Edvardsson, B., Eriksson, K., et al. 2008, *A&A*, 486, 951
- Hansen, C. J., Bergemann, M., Cescutti, G., et al. 2013, *Astronomy and Astrophysics*, 551, A57
- Hayek, W., Wiesendahl, U., Christlieb, N., et al. 2009, *A&A*, 504, 511
- Hill, V., Christlieb, N., Beers, T. C., et al. 2016, *ArXiv e-prints*
- Honda, S., Aoki, W., Kajino, T., et al. 2004, *ApJ*, 607, 474
- Idiart, T. & Thévenin, F. 2000, *ApJ*, 541, 207
- Izutani, N., Umeda, H., & Tominaga, N. 2009, *ApJ*, 692, 1517
- Jablonka, P., North, P., Mashonkina, L., et al. 2015, *A&A*, 583, A67
- Ji, A. P., Frebel, A., Simon, J. D., & Chiti, A. 2016, *ApJ*, 830, 93
- Kirby, E. N. & Cohen, J. G. 2012, *AJ*, 144, 168
- Kobayashi, C. & Nomoto, K. 2009, *The Astrophysical Journal*, 707, 1466
- Koposov, S. E., Gilmore, G., Walker, M. G., et al. 2011, *The Astrophysical Journal*, 736, 146
- Kratz, K.-L., Farouqi, K., Pfeiffer, B., et al. 2007, *ApJ*, 662, 39
- Kurucz, R. L. 2005, *Memorie della Societa Astronomica Italiana Supplementi*, 8, 14
- Lawler, J. E., Wickliffe, M. E., den Hartog, E. A., & Sneden, C. 2001, *ApJ*, 563, 1075
- Lodders, K., Plame, H., & Gail, H.-P. 2009, in *Landolt-Börnstein - Group VI Astronomy and Astrophysics Numerical Data and Functional Relationships in Science and Technology Volume 4B: Solar System*. Edited by J.E. Trümper, 2009, 4.4., 44–54
- Mashonkina, L. 2013, *A&A*, 550, A28
- Mashonkina, L. 2014, in *IAU Symposium*, Vol. 298, *IAU Symposium*, ed. S. Feltzing, G. Zhao, N. A. Walton, & P. Whitelock, 355–365
- Mashonkina, L., Christlieb, N., Barklem, P. S., et al. 2010, *A&A*, 516, A46
- Mashonkina, L. & Gehren, T. 2000, *A&A*, 364, 249
- Mashonkina, L. & Gehren, T. 2001, *A&A*, 376, 232
- Mashonkina, L., Gehren, T., & Bikmaev, I. 1999, *A&A*, 343, 519
- Mashonkina, L., Gehren, T., Shi, J.-R., Korn, A. J., & Grupp, F. 2011, *A&A*, 528, A87
- Mashonkina, L., Jablonka, P., Pakhomov, Y., Sitnova, T., & North, P. 2017, *A&A*, 604, A129, (Paper I)
- Mashonkina, L., Korn, A. J., & Przybilla, N. 2007, *A&A*, 461, 261
- Mashonkina, L., Sitnova, T., & Pakhomov, Y. 2016, *Astronomy Letters*, 42, 606
- Mashonkina, L., Zhao, G., Gehren, T., et al. 2008, *A&A*, 478, 529
- Mashonkina, L. I., Shimanskiĭ, V. V., & Sakhbullin, N. A. 2000, *Astronomy Reports*, 44, 790
- McConnachie, A. W. 2012, *The Astronomical Journal*, 144, 4
- McWilliam, A. 1998, *AJ*, 115, 1640
- Nishimura, N., Sawai, H., Takiwaki, T., Yamada, S., & Thielemann, F.-K. 2017, *ApJ*, 836, L21
- Nomoto, K., Kobayashi, C., & Tominaga, N. 2013, *Annual Review of Astronomy and Astrophysics*, 51, 457
- Norris, J. E., Yong, D., Gilmore, G., & Wyse, R. F. G. 2010, *ApJ*, 711, 350
- Okamoto, S., Arimoto, N., Yamada, Y., & Onodera, M. 2012, *The Astrophysical Journal*, 744, 96
- Pignatari, M., Gallino, R., Meynet, G., et al. 2008, *ApJ*, 687, L95
- Placco, V. M., Frebel, A., Beers, T. C., & Stancliffe, R. J. 2014, *ApJ*, 797, 21
- Raassen, A. J. J. & Uylings, P. H. M. 1998, *A&A*, 340, 300
- Raiteri, C. M., Busso, M., Picchio, G., Gallino, R., & Pulone, L. 1991, *ApJ*, 367, 228
- Reetz, J. K. 1991, *Diploma Thesis (Universität München)*
- Revaz, Y. & Jablonka, P. 2012, *Astronomy and Astrophysics*, 538, A82
- Roderick, T. A., Mackey, A. D., Jerjen, H., & Da Costa, G. S. 2016, *MNRAS*, 461, 3702
- Roederer, I. U. 2009, *The Astronomical Journal*, 137, 272
- Roederer, I. U. 2017, *ApJ*, 835, 23
- Roederer, I. U., Mateo, M., Bailey, III, J. I., et al. 2016, *AJ*, 151, 82
- Romano, D., Bellazzini, M., Starkenburg, E., & Leaman, R. 2015, *MNRAS*, 446, 4220
- Ryabchikova, T., Piskunov, N., Kurucz, R. L., et al. 2015, *Phys. Scr*, 90, 054005
- Ryabchikova, T., Piskunov, N., Pakhomov, Y., et al. 2016, *MNRAS*, 456, 1221
- Rybicki, G. B. & Hummer, D. G. 1991, *A&A*, 245, 171
- Rybicki, G. B. & Hummer, D. G. 1992, *A&A*, 262, 209
- Sakhbullin, N. A. 1983, *Trudy Kazanskaia Gorodkoj Astronomicheskoi Observatorii*, 48, 9
- Shi, J. R., Gehren, T., Butler, K., Mashonkina, L. I., & Zhao, G. 2008, *A&A*, 486, 303
- Shi, J. R., Gehren, T., Mashonkina, L., & Zhao, G. 2009, *A&A*, 503, 533
- Shimanskaya, N. N., Mashonkina, L. I., & Sakhbullin, N. A. 2000, *Astronomy Reports*, 44, 530
- Silverans, R. E., Borghs, G., Dumont, G., & van den Cruyce, J. M. 1980, *Zeitschrift für Physik A Hadrons and Nuclei*, 295, 311
- Simon, J. D., Frebel, A., McWilliam, A., Kirby, E. N., & Thompson, I. B. 2010, *ApJ*, 716, 446
- Simon, J. D., Jacobson, H. R., Frebel, A., et al. 2015, *ApJ*, 802, 93
- Siqueira Mello, C., Spite, M., Barbuy, B., et al. 2013, *A&A*, 550, A122
- Sitnova, T. M. 2016, *Astronomy Letters*, 42, 734
- Sitnova, T. M., Mashonkina, L. I., & Ryabchikova, T. A. 2016, *MNRAS*, 461, 1000
- Skúladóttir, Á., Tolstoy, E., Salvadori, S., et al. 2015, *A&A*, 574, A129
- Smith, G. 1981, *A&A*, 103, 351
- Sneden, C., Cowan, J. J., Lawler, J. E., et al. 2003, *ApJ*, 591, 936
- Spite, M., Andrievsky, S. M., Spite, F., et al. 2012, *A&A*, 541, A143
- Spite, M., Cayrel, R., Hill, V., et al. 2006, *A&A*, 455, 291
- Starkenburg, E., Hill, V., Tolstoy, E., et al. 2013, *A&A*, 549, A88
- Steenbock, W. & Holweger, H. 1984, *A&A*, 130, 319
- Tafelmeyer, M., Jablonka, P., Hill, V., et al. 2010, *A&A*, 524, A58
- Taubenberger, S., Benetti, S., Childress, M., et al. 2011, *Monthly Notices of the Royal Astronomical Society*, 412, 2735
- Travaglio, C., Galli, D., Gallino, R., et al. 1999, *ApJ*, 521, 691
- Truran, J. W., Cowan, J. J., Pilachowski, C. A., & Sneden, C. 2002, *PASP*, 114, 1293
- Tsujimoto, T. & Shigezumi, T. 2014, *A&A*, 565, L5
- Ural, U., Cescutti, G., Koch, A., et al. 2015, *MNRAS*, 449, 761
- Venn, K. A., Irwin, M., Shetrone, M. D., et al. 2004, *AJ*, 128, 1177
- Wanajo, S., Sekiguchi, Y., Nishimura, N., et al. 2014, *ApJ*, 789, L39
- Webster, D., Bland-Hawthorn, J., & Sutherland, R. 2015, *ApJ*, 799, L21
- Woolsey, S. E. & Hoffman, R. D. 1992, *ApJ*, 395, 202
- Zhao, G. & Gehren, T. 2000, *A&A*, 362, 1077
- Zhao, G., Mashonkina, L., Yan, H. L., et al. 2016, *ApJ*, 833, 225

Appendix A: Stellar abundances

Table A.1. Summary of the LTE and NLTE abundances of the investigated stars.

Z	Atom	N_l	LTE				NLTE			Method of analysis
			$\log \varepsilon$	$\sigma_{\log \varepsilon}$	[X/H]	[X/Fe]	$\log \varepsilon$	$\sigma_{\log \varepsilon}$	[X/Fe]	
Sculptor ET0381, $T_{\text{eff}} = 4570 \text{ K}$, $\log g = 1.17$, $[\text{Fe}/\text{H}] = -2.19$, $\xi_t = 1.7 \text{ km s}^{-1}$										
11	Na I	2	3.43	0.11	-2.90	-0.71	3.13	0.08	-1.01	W_{obs} (JNM15)
12	Mg I	3	4.98	0.07	-2.60	-0.41	5.00	0.07	-0.39	W_{obs} (JNM15)
13	Al I	1	2.72		-3.75	-1.56	2.82		-1.46	syn
14	Si I	2	4.80	0.04	-2.75	-0.56	4.79	0.01	-0.57	syn
20	Ca I	9	3.73	0.05	-2.63	-0.44	3.85	0.05	-0.32	W_{obs} (JNM15)
22	Ti I	10	2.09	0.17	-2.84	-0.65	2.31	0.15	-0.43	idem
22	Ti II	21	2.60	0.17	-2.33	-0.14	2.60	0.17	-0.14	idem
26	Fe I	73	5.14	0.17	-2.36	-0.17	5.23	0.17	-0.08	idem
26	Fe II	9	5.31	0.09	-2.19	0.00	5.31	0.09	0.00	idem
28	Ni I	1	3.75		-2.50	-0.31				idem
38	Sr II	1	-0.18		-3.08	-0.89	-0.13		-0.84	syn
56	Ba II	2	-1.52	0.02	-3.65	-1.46	-1.46	0.02	-1.40	syn
Sculptor 002_06, $T_{\text{eff}} = 4390 \text{ K}$, $\log g = 0.68$, $[\text{Fe}/\text{H}] = -3.11$, $\xi_t = 2.3 \text{ km s}^{-1}$										
11	Na I	2	2.72	0.16	-3.61	-0.50	2.60	0.11	-0.62	W_{obs} (JNM15)
12	Mg I	5	4.57	0.06	-3.01	0.10	4.59	0.06	0.12	W_{obs} (JNM15)
13	Al I	1	2.47		-4.00	-0.89	2.67		-0.69	syn
14	Si I	1	4.41		-3.14	-0.03	4.42		-0.02	syn
20	Ca I	5	3.35	0.03	-3.01	0.10	3.56	0.06	0.31	W_{obs} (JNM15)
22	Ti I	4	1.52	0.10	-3.41	-0.30	1.92	0.15	0.10	idem
22	Ti II	13	1.74	0.08	-3.19	-0.08	1.75	0.08	-0.07	idem
26	Fe I	69	4.12	0.17	-3.38	-0.27	4.33	0.16	-0.06	idem
26	Fe II	4	4.39	0.10	-3.11	0.00	4.39	0.09	0.00	idem
28	Ni I	1	2.89		-3.36	-0.25				idem
38	Sr II	1	-1.22		-4.12	-1.01	-1.03		-0.82	syn
Sculptor 031_11, $T_{\text{eff}} = 4670 \text{ K}$, $\log g = 1.13$, $[\text{Fe}/\text{H}] = -3.69$, $\xi_t = 2.0 \text{ km s}^{-1}$										
11	Na I	2	2.26	0.01	-4.07	-0.38	2.31	0.02	-0.33	W_{obs} (JNM15)
12	Mg I	4	4.05	0.13	-3.53	0.16	4.10	0.12	0.21	W_{obs} (JNM15)
13	Al I	2	1.93	0.08	-4.54	-0.85	2.48	0.01	-0.30	syn
14	Si I	1	4.31		-3.24	0.45	4.24		0.38	syn
20	Ca I	3	2.90	0.06	-3.46	0.23	3.18	0.05	0.51	W_{obs} (JNM15)
22	Ti I	3	1.74	0.24	-3.19	0.50	2.11	0.24	0.87	idem
22	Ti II	12	1.65	0.20	-3.30	0.39	1.72	0.20	0.46	idem
26	Fe I	37	3.82	0.15	-3.68	0.01	4.11	0.14	0.30	idem
26	Fe II	2	3.81	0.07	-3.69	0.00	3.81	0.07	0.00	idem
28	Ni I	2	2.44	0.16	-3.81	-0.12				idem
38	Sr II	2	-2.12	0.03	-5.02	-1.33	-1.80	0.03	-1.01	syn
Sculptor 074_02, $T_{\text{eff}} = 4680 \text{ K}$, $\log g = 1.23$, $[\text{Fe}/\text{H}] = -3.06$, $\xi_t = 2.0 \text{ km s}^{-1}$										
11	Na I	2	2.88	0.11	-3.45	-0.39	2.65	0.03	-0.62	W_{obs} (JNM15)
12	Mg I	5	4.58	0.10	-3.00	0.06	4.63	0.19	0.11	W_{obs} (JNM15)
13	Al I	1	2.57		-3.90	-0.84	2.75		-0.66	syn
14	Si I	2	5.02	0.05	-2.53	0.53	5.00	0.05	0.51	syn
20	Ca I	7	3.59	0.08	-2.77	0.29	3.80	0.14	0.50	W_{obs} (JNM15)
22	Ti I	4	1.82	0.20	-3.11	-0.05	2.15	0.20	0.28	idem
22	Ti II	17	1.84	0.22	-3.09	-0.03	1.85	0.23	-0.02	idem
26	Fe I	56	4.29	0.20	-3.21	-0.15	4.50	0.21	0.06	idem
26	Fe II	5	4.44	0.12	-3.06	0.00	4.44	0.12	0.00	idem
28	Ni I	2	3.12	0.00	-3.13	-0.07				idem
38	Sr II	2	-0.97	0.04	-3.87	-0.81	-0.91	0.04	-0.75	syn
Sculptor 03_059, $T_{\text{eff}} = 4530 \text{ K}$, $\log g = 1.08$, $[\text{Fe}/\text{H}] = -2.88$, $\xi_t = 1.9 \text{ km s}^{-1}$										
11	Na I	2	3.72	0.01	-2.61	0.27	3.34	0.02	-0.11	W_{obs} (JNM15)
12	Mg I	5	5.06	0.11	-2.52	0.36	5.06	0.11	0.36	W_{obs} (JNM15)
13	Al I	1	2.57		-3.90	-1.02	2.67		-0.92	syn
14	Si I	2	4.99	0.04	-2.56	0.32	4.98	0.04	0.31	syn
20	Ca I	9	3.60	0.08	-2.76	0.12	3.79	0.06	0.31	W_{obs} (JNM15)
22	Ti I	11	2.07	0.13	-2.86	0.02	2.35	0.12	0.30	idem
22	Ti II	19	2.34	0.18	-2.59	0.29	2.36	0.18	0.31	idem
26	Fe I	91	4.43	0.17	-3.07	-0.19	4.60	0.16	-0.02	idem

Table A.1. continued.

Z	Atom	N_l	LTE				NLTE			Method of analysis
			$\log \varepsilon$	$\sigma_{\log \varepsilon}$	[X/H]	[X/Fe]	$\log \varepsilon$	$\sigma_{\log \varepsilon}$	[X/Fe]	
26	Fe II	4	4.62	0.10	-2.88	0.00	4.62	0.10	0.00	idem
28	Ni I	3	3.14	0.11	-3.11	-0.23				idem
38	Sr II	1	-0.39		-3.29	-0.41	-0.31		-0.33	syn
56	Ba II	3	-1.23	0.04	-3.36	-0.48	-1.16	0.03	-0.41	syn
Sculptor 07-49, $T_{\text{eff}} = 4630$ K, $\log g = 1.28$, $[\text{Fe}/\text{H}] = -2.99$, $\xi_t = 2.0$ km s ⁻¹										
11	Na I	2	3.19	0.10	-3.14	-0.23	2.94	0.17	-0.48	W_{obs} (TJH10)
12	Mg I	2	4.99	0.01	-2.59	0.32	4.83	0.02	0.16	idem
20	Ca I	2	3.67	0.03	-2.69	0.22	3.82	0.04	0.37	idem
22	Ti I	6	2.08	0.19	-2.85	0.06	2.35	0.19	0.33	idem
22	Ti II	3	2.27	0.24	-2.66	0.25	2.29	0.23	0.27	idem
26	Fe I	22	4.46	0.17	-3.04	-0.13	4.64	0.15	0.05	idem
26	Fe II	4	4.59	0.15	-2.91	0.00	4.59	0.16	0.00	idem
28	Ni I	1	3.31	0.00	-2.94	-0.03				idem
Sculptor 07-50, $T_{\text{eff}} = 4800$ K, $\log g = 1.56$, $[\text{Fe}/\text{H}] = -4.0$, $\xi_t = 2.2$ km s ⁻¹										
11	Na I	2	2.37	0.05	-3.96	0.04	2.36	0.09	0.03	W_{obs} (TJH10)
12	Mg I	4	3.67	0.17	-3.91	0.09	3.87	0.08	0.29	W_{obs} (TJH10)
13	Al I	1	1.73		-4.74	-0.74	2.37		-0.10	syn
14	Si I	1	3.62		-3.93	0.07	3.60		0.05	syn
20	Ca II	1	2.86		-3.50	0.50	2.82		0.46	syn
22	Ti II	9	1.19	0.12	-3.74	0.26	1.29	0.13	0.36	W_{obs} (TJH10)
26	Fe I	16	3.59	0.11	-3.91	0.09	3.86	0.13	0.36	idem
26	Fe II	2	3.50	0.20	-4.00	0.00	3.50	0.20	0.00	idem
28	Ni I	2	1.93	0.10	-4.32	-0.32				idem
38	Sr II	2	-2.22	0.00	-5.12	-1.12	-1.99	0.00	-0.89	syn
56	Ba II	1	-2.66		-4.79	-0.79	-2.44		-0.57	syn
Sculptor 11_1_4296, $T_{\text{eff}} = 4810$ K, $\log g = 1.76$, $[\text{Fe}/\text{H}] = -3.70$, $\xi_t = 1.9$ km s ⁻¹										
11	Na I	2	2.34	0.08	-3.99	-0.29	2.31	0.13	-0.32	W_{obs} (SJF15)
12	Mg I	3	3.29	0.04	-4.29	-0.59	3.58	0.11	-0.30	W_{obs} (SJF15)
13	Al I	1	1.82		-4.65	-0.95	2.39		-0.38	syn
20	Ca II	1	2.56		-3.80	-0.10	2.62		-0.04	syn
22	Ti II	11	1.50	0.17	-3.43	0.27	1.56	0.16	0.33	W_{obs} (SJF15)
26	Fe I	21	3.59	0.37	-3.91	-0.21	3.82	0.41	0.02	idem
26	Fe II	2	3.80	0.00	-3.70	0.00	3.80	0.00	0.00	idem
Sculptor 6_6_402, $T_{\text{eff}} = 4890$ K, $\log g = 1.78$, $[\text{Fe}/\text{H}] = -3.66$, $\xi_t = 1.8$ km s ⁻¹										
11	Na I	2	2.63	0.08	-3.70	-0.04	2.59	0.03	-0.08	W_{obs} (SJF15)
12	Mg I	2	4.40	0.16	-3.18	0.48	4.43	0.10	0.51	W_{obs} (SJF15)
13	Al I	1	1.56	0.20	-4.91	-1.25	2.22	0.20	-0.59	syn
20	Ca II	1	3.00	0.20	-3.36	0.30	3.03	0.20	0.33	syn
22	Ti II	4	1.62	0.28	-3.31	0.35	1.68	0.29	0.41	W_{obs} (SJF15)
26	Fe I	20	3.95	0.33	-3.55	0.11	4.20	0.34	0.36	idem
26	Fe II	4	3.84	0.04	-3.66	0.00	3.84	0.04	0.00	idem
28	Ni I	2	2.74	0.15	-3.51	0.15				idem
38	Sr II	1	-1.51	0.00	-4.41	-0.75	-1.37	0.00	-0.61	syn
56	Ba II	1	-2.03	0.10	-4.16	-0.50	-1.82	0.10	-0.29	W_{obs} (SJF15)
Sculptor S1020549, $T_{\text{eff}} = 4650$ K, $\log g = 1.35$, $[\text{Fe}/\text{H}] = -3.67$, $\xi_t = 2.0$ km s ⁻¹										
11	Na I	2	2.48	0.01	-3.85	-0.18	2.42	0.08	-0.23	W_{obs} (SJF15)
12	Mg I	2	4.27	0.14	-3.31	0.36	4.28	0.07	0.37	W_{obs} (SJF15)
13	Al I	1	1.55	0.20	-4.92	-1.25	2.10	0.20	-0.70	syn
14	Si I	1	4.32	0.20	-3.23	0.44	4.26	0.20	0.38	syn
20	Ca I	2	2.98	0.08	-3.38	0.29	3.15	0.12	0.46	W_{obs} (SJF15)
22	Ti I	2	1.69	0.00	-3.24	0.43	2.01	0.03	0.75	idem
22	Ti II	16	1.62	0.22	-3.31	0.36	1.64	0.23	0.38	idem
26	Fe I	38	3.71	0.22	-3.79	-0.12	3.99	0.27	0.16	idem
26	Fe II	5	3.83	0.15	-3.67	0.00	3.83	0.15	0.00	idem
28	Ni I	1	2.59	0.00	-3.66	0.01				idem
Sculptor 1019417, $T_{\text{eff}} = 4280$ K, $\log g = 0.50$, $[\text{Fe}/\text{H}] = -2.48$, $\xi_t = 2.0$ km s ⁻¹										
11	Na I	2	3.16	0.00	-3.17	-0.69	3.16	0.00	-0.69	W_{obs} (KC12)
12	Mg I	5	5.76	0.22	-1.82	0.66	5.73	0.08	0.63	idem

Table A.1. continued.

Z	Atom	N_l	LTE				NLTE			Method of analysis
			$\log \varepsilon$	$\sigma_{\log \varepsilon}$	[X/H]	[X/Fe]	$\log \varepsilon$	$\sigma_{\log \varepsilon}$	[X/Fe]	
13	Al I	1	3.50	0.20	-2.97	-0.49	3.70	0.20	-0.29	idem
20	Ca I	13	4.16	0.11	-2.20	0.28	4.34	0.11	0.46	idem
22	Ti I	8	2.46	0.16	-2.47	0.01	2.90	0.13	0.45	idem
22	Ti II	5	2.97	0.09	-1.96	0.52	2.98	0.09	0.53	idem
26	Fe I	32	5.00	0.17	-2.50	-0.02	5.12	0.16	0.10	idem
26	Fe II	10	5.02	0.18	-2.48	0.00	5.02	0.18	0.00	idem
28	Ni I	5	3.80	0.05	-2.45	0.03				idem
38	Sr II	1	0.19		-2.71	-0.23	0.39		-0.03	idem
56	Ba II	3	-0.85	0.07	-2.98	-0.50	-0.85	0.02	-0.50	idem
63	Eu II	1	-2.25		-2.76	-0.28	-2.13		-0.16	idem
Fornax 05-42, $T_{\text{eff}} = 4325$ K, $\log g = 0.70$, $[\text{Fe}/\text{H}] = -3.37$, $\xi_t = 2.3$ km s $^{-1}$										
11	Na I	2	2.70	0.06	-3.63	-0.26	2.51	0.10	-0.45	W_{obs} (TJH10)
12	Mg I	3	4.51	0.10	-3.07	0.30	4.46	0.14	0.25	W_{obs} (TJH10)
13	Al I	1	2.07		-4.40	-1.03	2.37		-0.73	syn
14	Si I	2	4.30	0.00	-3.25	0.12	4.28	0.00	0.10	syn
20	Ca I	3	3.24	0.29	-3.12	0.25	3.43	0.22	0.44	W_{obs} (TJH10)
22	Ti I	3	1.32	0.07	-3.61	-0.24	1.68	0.06	0.12	idem
22	Ti II	6	1.76	0.05	-3.17	0.20	1.78	0.04	0.22	idem
26	Fe I	20	3.83	0.19	-3.67	-0.30	4.03	0.17	-0.10	idem
26	Fe II	2	4.13	0.08	-3.37	0.00	4.13	0.08	0.00	idem
28	Ni I	1	2.43		-3.82	-0.45				idem
38	Sr II	2	-0.26	0.03	-3.16	0.21	-0.06	0.03	0.41	syn
56	Ba II	2	-1.93	0.02	-4.06	-0.69	-1.79	0.07	-0.55	syn
Sextans 11-04, $T_{\text{eff}} = 4380$ K, $\log g = 0.57$, $[\text{Fe}/\text{H}] = -2.60$, $\xi_t = 2.2$ km s $^{-1}$										
11	Na I	2	3.48	0.02	-2.85	-0.25	3.33	0.03	-0.40	W_{obs} (TJH10)
12	Mg I	3	5.17	0.02	-2.41	0.19	5.22	0.07	0.24	W_{obs} (TJH10)
13	Al I	1	3.12	0.20	-3.35	-0.75	3.32	0.20	-0.55	syn
14	Si I	1	5.16	0.00	-2.39	0.21	5.16	0.00	0.21	syn
20	Ca I	6	3.75	0.16	-2.61	-0.01	3.90	0.16	0.14	W_{obs} (TJH10)
22	Ti I	7	2.02	0.06	-2.91	-0.31	2.49	0.13	0.16	idem
22	Ti II	7	2.40	0.10	-2.53	0.07	2.42	0.10	0.09	idem
26	Fe I	37	4.68	0.14	-2.82	-0.22	4.84	0.13	-0.06	idem
26	Fe II	4	4.90	0.12	-2.60	0.00	4.90	0.12	0.00	idem
28	Ni I	1	3.22		-3.03	-0.43				idem
38	Sr II	2	-0.39	0.15	-3.29	-0.69	-0.21	0.14	-0.51	syn
56	Ba II	2	-1.59	0.00	-3.72	-1.12	-1.49	0.05	-1.02	syn
Sextans 24-72, $T_{\text{eff}} = 4400$ K, $\log g = 0.76$, $[\text{Fe}/\text{H}] = -2.84$, $\xi_t = 2.2$ km s $^{-1}$										
11	Na I	2	4.48	0.11	-1.85	0.99	4.34	0.06	0.85	W_{obs} (TJH10)
12	Mg I	3	4.86	0.05	-2.72	0.12	4.91	0.07	0.17	W_{obs} (TJH10)
13	Al I	1	2.76		-3.71	-0.87	2.96		-0.67	syn
14	Si I	1	4.69	0.00	-2.86	-0.02	4.69	0.00	-0.02	syn
20	Ca I	4	3.59	0.10	-2.77	0.07	3.77	0.14	0.25	W_{obs} (TJH10)
22	Ti I	6	1.85	0.08	-3.08	-0.24	2.22	0.10	0.13	idem
22	Ti II	7	2.23	0.10	-2.70	0.14	2.24	0.10	0.15	idem
26	Fe I	43	4.55	0.14	-2.95	-0.11	4.71	0.14	0.05	idem
26	Fe II	3	4.66	0.05	-2.84	0.00	4.66	0.05	0.00	idem
28	Ni I	1	3.33		-2.92	-0.08				idem
38	Sr II	1	-0.54		-3.44	-0.60	-0.37		-0.43	syn
56	Ba II	1	-1.92	0.00	-4.05	-1.21	-1.79	0.00	-1.08	syn
Ursa Minor 396, $T_{\text{eff}} = 4320$ K, $\log g = 0.70$, $[\text{Fe}/\text{H}] = -2.26$, $\xi_t = 2.5$ km s $^{-1}$										
12	Mg I	3	5.48	0.18	-2.10	0.16	5.40	0.18	0.08	W_{obs} (UCK15)
20	Ca I	9	4.18	0.16	-2.18	0.08	4.30	0.18	0.20	idem
22	Ti I	8	2.75	0.26	-2.18	0.08	3.10	0.28	0.43	idem
22	Ti II	10	2.92	0.29	-2.01	0.25	2.92	0.29	0.25	idem
26	Fe I	26	5.04	0.14	-2.46	-0.20	5.13	0.14	-0.11	idem
26	Fe II	5	5.24	0.05	-2.26	0.00	5.24	0.05	0.00	idem
28	Ni I	5	3.80	0.13	-2.45	-0.19				idem
Ursa Minor 446, $T_{\text{eff}} = 4600$ K, $\log g = 1.37$, $[\text{Fe}/\text{H}] = -2.52$, $\xi_t = 2.5$ km s $^{-1}$										
12	Mg I	2	5.27	0.12	-2.31	0.21	5.41	0.03	0.35	W_{obs} (UCK15)

Table A.1. continued.

Z	Atom	N_l	LTE				NLTE			Method of analysis
			$\log \varepsilon$	$\sigma_{\log \varepsilon}$	[X/H]	[X/Fe]	$\log \varepsilon$	$\sigma_{\log \varepsilon}$	[X/Fe]	
20	Ca I	5	4.03	0.28	-2.33	0.19	4.07	0.28	0.23	idem
22	Ti I	4	2.76	0.25	-2.17	0.35	3.00	0.27	0.59	idem
22	Ti II	7	2.95	0.43	-1.98	0.54	2.96	0.44	0.55	idem
26	Fe I	28	4.88	0.27	-2.62	-0.10	5.00	0.27	0.02	idem
26	Fe II	3	4.98	0.28	-2.52	0.00	4.98	0.28	0.00	idem
28	Ni I	1	3.90	0.20	-2.35	0.17				idem
Ursa Minor 718, $T_{\text{eff}} = 4630$ K, $\log g = 1.13$, $[\text{Fe}/\text{H}] = -2.00$, $\xi_t = 2.0$ km s $^{-1}$										
12	Mg I	3	5.77	0.06	-1.81	0.19	5.81	0.21	0.23	W_{obs} (UCK15)
20	Ca I	10	4.54	0.18	-1.82	0.18	4.63	0.26	0.27	idem
22	Ti I	6	2.92	0.12	-2.01	-0.01	3.16	0.11	0.23	idem
22	Ti II	6	3.15	0.18	-1.78	0.22	3.15	0.18	0.22	idem
26	Fe I	32	5.45	0.19	-2.05	-0.05	5.56	0.18	0.06	idem
26	Fe II	3	5.50	0.12	-2.00	0.00	5.50	0.12	0.00	idem
28	Ni I	6	4.18	0.12	-2.07	-0.07				idem
Ursa Minor 20103, $T_{\text{eff}} = 4780$ K, $\log g = 1.55$, $[\text{Fe}/\text{H}] = -3.09$, $\xi_t = 2.0$ km s $^{-1}$										
11	Na I	2	3.19	0.26	-3.14	-0.05	2.94	0.17	-0.30	W_{obs} (KC12)
12	Mg I	4	4.85	0.02	-2.73	0.36	4.91	0.10	0.42	idem
13	Al I	1	2.09	0.20	-4.38	-1.29	2.44	0.20	-0.94	idem
14	Si I	1	4.34	0.00	-3.21	-0.12	4.31	0.00	-0.15	idem
20	Ca I	4	3.40	0.11	-2.96	0.13	3.62	0.06	0.35	idem
22	Ti I	2	1.87	0.17	-3.06	0.03	2.20	0.18	0.36	idem
22	Ti II	4	1.89	0.18	-3.04	0.05	1.91	0.23	0.07	idem
26	Fe I	34	4.33	0.14	-3.17	-0.08	4.53	0.14	0.12	idem
26	Fe II	7	4.41	0.17	-3.09	0.00	4.41	0.17	0.00	idem
38	Sr II	2	-1.05	0.06	-3.95	-0.86	-1.03	0.05	-0.84	idem
56	Ba II	2	-1.71	0.26	-3.84	-0.75	-1.59	0.23	-0.63	idem
Ursa Minor COS233, $T_{\text{eff}} = 4370$ K, $\log g = 0.77$, $[\text{Fe}/\text{H}] = -2.23$, $\xi_t = 2.0$ km s $^{-1}$										
11	Na I	2	3.68	0.01	-2.65	-0.42	3.54	0.03	-0.56	W_{obs} (CH10)
12	Mg I	5	5.65	0.10	-1.93	0.30	5.63	0.01	0.28	idem
13	Al I	1	3.38	0.30	-3.09	-0.86	3.48	0.30	-0.76	idem
20	Ca I	13	4.17	0.09	-2.19	0.04	4.31	0.10	0.18	idem
22	Ti I	9	2.51	0.11	-2.42	-0.19	2.86	0.14	0.16	idem
22	Ti II	5	3.12	0.21	-1.81	0.42	3.12	0.21	0.42	idem
26	Fe I	29	5.14	0.11	-2.36	-0.13	5.23	0.11	-0.04	idem
26	Fe II	8	5.27	0.11	-2.23	0.00	5.27	0.11	0.00	idem
28	Ni I	4	3.85	0.04	-2.40	-0.17				idem
38	Sr II	1	0.15	0.20	-2.75	-0.52	0.23	0.20	-0.44	idem
56	Ba II	3	-0.26	0.06	-2.39	-0.16	-0.31	0.11	-0.21	idem
Ursa Minor 28104, $T_{\text{eff}} = 4275$ K, $\log g = 0.65$, $[\text{Fe}/\text{H}] = -2.12$, $\xi_t = 2.0$ km s $^{-1}$										
11	Na I	2	3.76	0.22	-2.57	-0.45	3.71	0.24	-0.50	W_{obs} (CH10)
12	Mg I	5	5.70	0.17	-1.88	0.24	5.67	0.07	0.21	idem
13	Al I	1	3.58	0.30	-2.89	-0.77	3.70	0.30	-0.65	idem
20	Ca I	14	4.12	0.09	-2.24	-0.12	4.27	0.09	0.03	idem
22	Ti I	9	2.33	0.12	-2.60	-0.48	2.73	0.11	-0.08	idem
22	Ti II	6	3.06	0.11	-1.87	0.25	3.06	0.11	0.25	idem
26	Fe I	25	5.15	0.13	-2.35	-0.23	5.23	0.13	-0.15	idem
26	Fe II	6	5.38	0.07	-2.12	0.00	5.38	0.07	0.00	idem
28	Ni I	4	3.96	0.05	-2.29	-0.17				idem
38	Sr II	1	0.29	0.00	-2.61	-0.49	0.42	0.00	-0.36	idem
56	Ba II	3	-0.94	0.02	-3.07	-0.95	-0.92	0.01	-0.93	idem
63	Eu II	1	-2.25		-2.76	-0.28	-2.13		-0.16	idem
Ursa Minor 41065, $T_{\text{eff}} = 4350$ K, $\log g = 0.63$, $[\text{Fe}/\text{H}] = -2.48$, $\xi_t = 2.0$ km s $^{-1}$										
11	Na I	2	3.60	0.05	-2.73	-0.25	3.49	0.04	-0.36	W_{obs} (CH10)
12	Mg I	4	5.57	0.15	-2.01	0.47	5.57	0.11	0.47	idem
14	Si I	1	5.12	0.00	-2.43	0.05	5.12	0.00	0.05	idem
20	Ca I	11	4.00	0.11	-2.36	0.12	4.19	0.12	0.31	idem
22	Ti I	9	2.23	0.14	-2.70	-0.22	2.67	0.17	0.22	idem
22	Ti II	6	2.87	0.19	-2.06	0.42	2.88	0.19	0.43	idem
26	Fe I	34	4.92	0.11	-2.58	-0.10	5.05	0.11	0.03	idem

Table A.1. continued.

Z	Atom	N_l	LTE				NLTE			Method of analysis
			$\log \varepsilon$	$\sigma_{\log \varepsilon}$	[X/H]	[X/Fe]	$\log \varepsilon$	$\sigma_{\log \varepsilon}$	[X/Fe]	
26	Fe II	7	5.02	0.17	-2.48	0.00	5.02	0.17	0.00	idem
28	Ni I	5	3.60	0.05	-2.65	-0.17				idem
38	Sr II	1	0.19	0.00	-2.71	-0.23	0.36	0.00	-0.06	idem
56	Ba II	3	-0.58	0.08	-2.71	-0.23	-0.62	0.03	-0.27	idem
63	Eu II	1	-1.57		-2.08	0.40	-1.44		0.53	idem
Ursa Minor JI19, $T_{\text{eff}} = 4530$ K, $\log g = 1.00$, $[\text{Fe}/\text{H}] = -3.02$, $\xi_t = 2.0$ km s $^{-1}$										
11	Na I	2	3.22	0.08	-3.11	-0.09	2.98	0.02	-0.33	W_{obs} (CH10)
12	Mg I	4	4.89	0.03	-2.69	0.33	4.92	0.11	0.36	idem
13	Al I	1	3.07	0.20	-3.40	-0.38	3.14	0.20	-0.31	idem
14	Si I	2	5.00	0.08	-2.55	0.47	5.05	0.15	0.52	idem
20	Ca I	9	3.58	0.13	-2.78	0.24	3.78	0.15	0.44	idem
22	Ti I	4	2.14	0.04	-2.79	0.23	2.47	0.06	0.56	idem
22	Ti II	5	2.32	0.18	-2.61	0.41	2.33	0.18	0.42	idem
26	Fe I	42	4.32	0.22	-3.18	-0.16	4.50	0.22	0.02	idem
26	Fe II	9	4.48	0.15	-3.02	0.00	4.48	0.15	0.00	idem
28	Ni I	2	3.12	0.06	-3.13	-0.11				idem
38	Sr II	1	-0.28	0.00	-3.18	-0.16	-0.18	0.00	-0.06	idem
56	Ba II	2	-1.96	0.32	-4.09	-1.07	-1.82	0.36	-0.93	idem
63	Eu II	1	-2.13		-2.64	0.38	-1.94		0.57	idem
Ursa Minor 33533, $T_{\text{eff}} = 4430$ K, $\log g = 0.75$, $[\text{Fe}/\text{H}] = -3.14$, $\xi_t = 2.0$ km s $^{-1}$										
11	Na I	2	2.84	0.08	-3.49	-0.35	2.66	0.03	-0.53	W_{obs} (CH10)
12	Mg I	4	4.68	0.06	-2.90	0.24	4.73	0.09	0.29	idem
13	Al I	1	3.04	0.20	-3.43	-0.29	3.18	0.20	-0.15	idem
14	Si I	1	4.21	0.00	-3.34	-0.20	4.21	0.00	-0.20	idem
20	Ca I	6	3.12	0.20	-3.24	-0.10	3.36	0.11	0.14	idem
22	Ti I	6	1.56	0.10	-3.37	-0.23	1.96	0.09	0.17	idem
22	Ti II	9	1.89	0.14	-3.04	0.10	1.91	0.15	0.12	idem
26	Fe I	42	4.14	0.16	-3.36	-0.22	4.33	0.16	-0.03	idem
26	Fe II	10	4.36	0.12	-3.14	0.00	4.36	0.12	0.00	idem
28	Ni I	2	2.81	0.10	-3.44	-0.30				idem
38	Sr II	1	-0.05	0.00	-2.95	0.19	0.13	0.00	0.37	idem
56	Ba II	2	-2.01	0.07	-4.14	-1.00	-1.86	0.12	-0.85	idem
63	Eu II	1	-2.40		-2.91	0.23	-2.19		0.44	idem
Ursa Minor 36886, $T_{\text{eff}} = 4400$ K, $\log g = 0.82$, $[\text{Fe}/\text{H}] = -2.56$, $\xi_t = 2.0$ km s $^{-1}$										
11	Na I	2	3.60	0.10	-2.73	-0.17	3.40	0.11	-0.37	W_{obs} (CH10)
12	Mg I	5	5.32	0.06	-2.26	0.30	5.33	0.05	0.31	idem
13	Al I	1	2.49	0.20	-3.98	-1.42	2.65	0.20	-1.26	idem
14	Si I	1	5.00	0.00	-2.55	0.01	5.00	0.00	0.01	idem
20	Ca I	12	3.89	0.12	-2.47	0.09	4.05	0.12	0.25	idem
22	Ti I	9	2.18	0.10	-2.75	-0.19	2.52	0.15	0.15	idem
22	Ti II	6	2.78	0.08	-2.15	0.41	2.79	0.08	0.42	idem
26	Fe I	40	4.80	0.15	-2.70	-0.14	4.92	0.15	-0.02	idem
26	Fe II	8	4.94	0.09	-2.56	0.00	4.94	0.09	0.00	idem
28	Ni I	5	3.58	0.10	-2.67	-0.11				idem
38	Sr II	1	0.03	0.00	-2.87	-0.31	0.17	0.00	-0.17	idem
56	Ba II	3	-0.64	0.06	-2.77	-0.21	-0.68	0.08	-0.25	idem
63	Eu II	1	-1.58		-2.09	0.47	-1.45		0.60	idem
Boötes I 033, $T_{\text{eff}} = 4730$ K, $\log g = 1.4$, $[\text{Fe}/\text{H}] = -2.28$, $\xi_t = 2.3$ km s $^{-1}$										
11	Na I	1	4.03		-2.30	-0.04	3.51		-0.56	W_{obs} (GNM13)
12	Mg I	1	5.68		-1.90	0.36	5.61		0.29	idem
20	Ca I	8	4.17	0.18	-2.19	0.07	4.30	0.22	0.20	idem
22	Ti I	5	2.52	0.27	-2.41	-0.15	2.73	0.30	0.06	idem
22	Ti II	3	2.74	0.23	-2.19	0.07	2.74	0.23	0.07	idem
26	Fe I	33	5.18	0.17	-2.32	-0.06	5.29	0.17	0.05	idem
26	Fe II	4	5.24	0.16	-2.26	0.00	5.24	0.16	0.00	idem
28	Ni I	3	3.82	0.14	-2.43	-0.17				idem
56	Ba II	3	-0.73	0.15	-2.86	-0.60	-0.73	0.19	-0.60	idem
Boötes I 041, $T_{\text{eff}} = 4750$ K, $\log g = 1.6$, $[\text{Fe}/\text{H}] = -1.54$, $\xi_t = 2.0$ km s $^{-1}$										
12	Mg I	1	6.63		-0.95	0.59	6.46		0.42	W_{obs} (GNM13)

Table A.1. continued.

Z	Atom	N_l	LTE				NLTE			Method of analysis
			$\log \varepsilon$	$\sigma_{\log \varepsilon}$	[X/H]	[X/Fe]	$\log \varepsilon$	$\sigma_{\log \varepsilon}$	[X/Fe]	
20	Ca I	9	4.87	0.29	-1.49	0.05	4.93	0.29	0.11	idem
22	Ti I	2	4.01	0.12	-0.92	0.62	4.17	0.14	0.78	idem
22	Ti II	1	4.19		-0.74	0.80	4.19		0.80	idem
26	Fe I	16	5.79	0.23	-1.71	-0.17	5.86	0.23	-0.10	idem
26	Fe II	2	5.96	0.07	-1.54	0.00	5.96	0.07	0.00	idem
28	Ni I	1	4.19		-2.06	-0.52				idem
56	Ba II	2	-0.02	0.15	-2.15	-0.61	-0.13	0.15	-0.72	idem
Boötes I 094, $T_{\text{eff}} = 4570$ K, $\log g = 1.01$, $[\text{Fe}/\text{H}] = -2.69$, $\xi_t = 2.2$ km s $^{-1}$										
11	Na I	1	3.54	0.20	-2.79	-0.10	3.27	0.20	-0.37	W_{obs} (GNM13)
12	Mg I	1	5.26	0.20	-2.32	0.37	5.27	0.20	0.38	idem
20	Ca I	6	3.70	0.09	-2.66	0.03	3.84	0.06	0.17	idem
22	Ti I	6	2.16	0.11	-2.77	-0.08	2.44	0.13	0.20	idem
22	Ti II	5	2.33	0.10	-2.60	0.09	2.35	0.10	0.11	idem
26	Fe I	41	4.55	0.16	-2.95	-0.26	4.72	0.15	-0.09	idem
26	Fe II	2	4.81	0.08	-2.69	0.00	4.81	0.08	0.00	idem
28	Ni I	3	3.33	0.16	-2.92	-0.23				idem
56	Ba II	2	-1.74	0.40	-3.87	-1.18	-1.61	0.46	-1.05	idem
Boötes I 117, $T_{\text{eff}} = 4700$ K, $\log g = 1.4$, $[\text{Fe}/\text{H}] = -2.16$, $\xi_t = 2.3$ km s $^{-1}$										
12	Mg I	1	5.50		-2.08	0.01	5.47		-0.02	W_{obs} (GNM13)
20	Ca I	11	4.30	0.13	-2.06	0.03	4.38	0.16	0.11	idem
22	Ti I	6	2.73	0.09	-2.20	-0.11	2.93	0.11	0.09	idem
22	Ti II	4	2.86	0.14	-2.07	0.02	2.86	0.14	0.02	idem
26	Fe I	33	5.25	0.19	-2.25	-0.16	5.35	0.19	-0.06	idem
26	Fe II	3	5.41	0.23	-2.09	0.00	5.41	0.23	0.00	idem
28	Ni I	3	3.90	0.22	-2.35	-0.26				idem
56	Ba II	3	-0.85	0.42	-2.98	-0.89	-0.77	0.46	-0.81	idem
Boötes I 127, $T_{\text{eff}} = 4670$ K, $\log g = 1.4$, $[\text{Fe}/\text{H}] = -2.01$, $\xi_t = 2.3$ km s $^{-1}$										
11	Na I	2	3.92	0.01	-2.41	-0.48	3.50	0.01	-0.90	W_{obs} (FNG16)
12	Mg I	3	5.62	0.12	-1.96	-0.03	5.64	0.01	-0.01	W_{obs} (FNG16)
13	Al I	1	3.35		-3.12	-1.19	3.40		-1.14	syn
14	Si I	1	5.97		-1.58	0.35	5.97		0.35	syn
20	Ca I	11	4.42	0.10	-1.94	-0.01	4.51	0.11	0.09	W_{obs} (FNG16)
22	Ti I	7	3.01	0.25	-1.92	0.01	3.20	0.27	0.20	idem
22	Ti II	3	3.09	0.02	-1.84	0.09	3.09	0.02	0.09	idem
26	Fe I	19	5.40	0.18	-2.10	-0.17	5.50	0.18	-0.07	idem
26	Fe II	3	5.57	0.03	-1.93	0.00	5.57	0.03	0.00	idem
28	Ni I	2	4.20	0.05	-2.05	-0.12				idem
38	Sr II	1	-0.50	0.10	-3.40	-1.47	-0.50	0.10	-1.47	syn
56	Ba II	2	-0.62	0.02	-2.75	-0.82	-0.59	0.01	-0.79	syn
Boötes I 130, $T_{\text{eff}} = 4730$ K, $\log g = 1.4$, $[\text{Fe}/\text{H}] = -2.20$, $\xi_t = 2.3$ km s $^{-1}$										
11	Na I	1	3.94		-2.39	-0.19	3.42		-0.71	W_{obs} (GNM13)
12	Mg I	1	5.56		-2.02	0.18	5.49		0.11	idem
20	Ca I	6	4.10	0.22	-2.26	-0.06	4.17	0.19	0.01	idem
22	Ti I	3	2.51	0.12	-2.42	-0.22	2.72	0.15	-0.01	idem
22	Ti II	3	2.92	0.14	-2.01	0.19	2.92	0.14	0.19	idem
26	Fe I	32	5.15	0.18	-2.35	-0.15	5.26	0.18	-0.04	idem
26	Fe II	2	5.30	0.06	-2.20	0.00	5.30	0.06	0.00	idem
28	Ni I	3	3.90	0.11	-2.35	-0.15				idem
56	Ba II	3	-0.87	0.42	-3.00	-0.80	-0.81	0.44	-0.74	
Boötes I 980, $T_{\text{eff}} = 4760$ K, $\log g = 1.8$, $[\text{Fe}/\text{H}] = -2.94$, $\xi_t = 1.8$ km s $^{-1}$										
11	Na I	2	3.50	0.06	-2.83	0.11	3.09	0.01	-0.30	W_{obs} (FNG16)
12	Mg I	3	4.92	0.05	-2.66	0.28	5.08	0.11	0.44	W_{obs} (FNG16)
13	Al I	1	2.86	0.20	-3.61	-0.67	3.10	0.20	-0.43	syn
14	Si I	1	5.04	0.20	-2.51	0.43	5.01	0.20	0.40	syn
20	Ca I	5	3.65	0.15	-2.71	0.23	3.81	0.15	0.39	W_{obs} (FNG16)
22	Ti I	5	2.34	0.13	-2.59	0.35	2.57	0.13	0.58	idem
22	Ti II	23	2.52	0.18	-2.41	0.53	2.52	0.18	0.53	idem
26	Fe I	49	4.49	0.19	-3.01	-0.07	4.59	0.19	0.03	idem
26	Fe II	9	4.56	0.19	-2.94	0.00	4.56	0.19	0.00	idem

Table A.1. continued.

Z	Atom	N_l	LTE				NLTE			Method of analysis
			$\log \varepsilon$	$\sigma_{\log \varepsilon}$	[X/H]	[X/Fe]	$\log \varepsilon$	$\sigma_{\log \varepsilon}$	[X/Fe]	
28	Ni I	3	3.38	0.19	-2.87	0.07				idem
38	Sr II	1	-0.98	0.20	-3.88	-0.94	-0.96	0.20	-0.92	syn
56	Ba II	2	-1.77	0.01	-3.90	-0.96	-1.62	0.04	-0.81	syn
Boötes I 1137, $T_{\text{eff}} = 4700$ K, $\log g = 1.39$, $[\text{Fe}/\text{H}] = -3.76$, $\xi_t = 1.9$ km s $^{-1}$										
11	Na I	2	2.46	0.05	-3.87	-0.11	2.40	0.10	-0.17	W_{obs} (NYG10)
12	Mg I	5	4.28	0.10	-3.30	0.46	4.29	0.11	0.47	idem
13	Al I	1	2.14		-4.33	-0.57	2.48		-0.23	idem
14	Si I	1	4.25		-3.30	0.46	4.18		0.39	idem
20	Ca I	7	3.16	0.09	-3.20	0.56	3.38	0.16	0.78	idem
22	Ti I	5	1.76	0.07	-3.17	0.59	2.10	0.10	0.93	idem
22	Ti II	17	1.91	0.15	-3.02	0.74	1.93	0.15	0.76	idem
26	Fe I	39	3.75	0.18	-3.75	0.01	4.01	0.16	0.27	idem
26	Fe II	2	3.74	0.06	-3.76	0.00	3.74	0.06	0.00	idem
28	Ni I	3	2.49	0.15	-3.76	0.00				idem
38	Sr II	2	-2.05	0.06	-4.95	-1.19	-1.83	0.01	-0.97	idem
56	Ba II	1	-2.22		-4.35	-0.59	-2.08		-0.45	idem
UMa II S1, $T_{\text{eff}} = 4850$ K, $\log g = 2.05$, $[\text{Fe}/\text{H}] = -2.96$, $\xi_t = 1.8$ km s $^{-1}$										
11	Na I	2	3.08	0.05	-3.25	-0.29	2.84	0.03	-0.53	W_{obs} (FSG10)
12	Mg I	5	4.79	0.18	-2.79	0.17	4.89	0.26	0.27	idem
20	Ca I	7	3.53	0.23	-2.83	0.13	3.68	0.24	0.28	idem
22	Ti I	3	2.02	0.22	-2.91	0.05	2.27	0.23	0.30	idem
22	Ti II	9	2.10	0.25	-2.83	0.13	2.11	0.25	0.14	idem
26	Fe I	35	4.34	0.17	-3.16	-0.20	4.47	0.18	-0.07	idem
26	Fe II	7	4.54	0.14	-2.96	0.00	4.54	0.14	0.00	idem
28	Ni I	2	3.46	0.40	-2.79	0.17				idem
38	Sr II	1	-1.08	0.10	-3.98	-1.02	-0.97	0.10	-0.91	idem
56	Ba II	1	-2.09	0.10	-4.22	-1.26	-1.95	0.10	-1.12	idem
UMa II S2, $T_{\text{eff}} = 4780$ K, $\log g = 1.83$, $[\text{Fe}/\text{H}] = -2.94$, $\xi_t = 2.0$ km s $^{-1}$										
11	Na I	2	3.09	0.08	-3.24	-0.30	2.85	0.16	-0.54	W_{obs} (FSG10)
12	Mg I	5	4.77	0.08	-2.81	0.13	4.89	0.26	0.25	idem
20	Ca I	7	3.52	0.19	-2.84	0.10	3.70	0.17	0.28	idem
22	Ti I	4	2.00	0.19	-2.93	0.01	2.24	0.19	0.25	idem
22	Ti II	9	2.13	0.37	-2.80	0.14	2.13	0.39	0.14	idem
26	Fe I	24	4.31	0.16	-3.19	-0.25	4.46	0.15	-0.10	idem
26	Fe II	6	4.56	0.18	-2.94	0.00	4.56	0.18	0.00	idem
38	Sr II	1	-1.34	0.10	-4.24	-1.30	-1.19	0.10	-1.15	idem
56	Ba II	2	-1.69	0.12	-3.82	-0.88	-1.57	0.15	-0.76	idem
UMa II S3, $T_{\text{eff}} = 4560$ K, $\log g = 1.34$, $[\text{Fe}/\text{H}] = -2.26$, $\xi_t = 1.8$ km s $^{-1}$										
11	Na I	2	3.73	0.01	-2.60	-0.34	3.35	0.01	-0.72	W_{obs} (FSG10)
12	Mg I	4	5.91	0.15	-1.67	0.59	5.89	0.07	0.57	idem
20	Ca I	15	4.54	0.18	-1.82	0.44	4.64	0.18	0.54	idem
22	Ti I	12	2.52	0.10	-2.41	-0.15	2.74	0.08	0.07	idem
22	Ti II	11	2.79	0.14	-2.14	0.12	2.80	0.14	0.13	idem
26	Fe I	45	5.07	0.14	-2.43	-0.17	5.16	0.14	-0.08	idem
26	Fe II	11	5.24	0.10	-2.26	0.00	5.24	0.10	0.00	idem
28	Ni I	5	3.73	0.09	-2.52	-0.26				idem
38	Sr II	1	-0.68	0.10	-3.58	-1.32	-0.64	0.10	-1.28	idem
56	Ba II	2	-0.50	0.05	-2.63	-0.37	-0.52	0.10	-0.39	idem
Leo IV S1, $T_{\text{eff}} = 4530$ K, $\log g = 1.09$, $[\text{Fe}/\text{H}] = -2.58$, $\xi_t = 2.2$ km s $^{-1}$										
11	Na I	2	3.62	0.37	-2.71	-0.13	3.26	0.35	-0.49	W_{obs} (SFM10)
12	Mg I	5	5.06	0.15	-2.52	0.06	5.11	0.11	0.11	idem
20	Ca I	5	3.64	0.14	-2.72	-0.14	3.81	0.07	0.03	idem
22	Ti I	2	2.14	0.21	-2.79	-0.21	2.43	0.23	0.08	idem
22	Ti II	9	2.27	0.22	-2.66	-0.08	2.27	0.23	-0.08	idem
26	Fe I	32	4.68	0.21	-2.82	-0.24	4.80	0.22	-0.12	idem
26	Fe II	4	4.92	0.13	-2.58	0.00	4.92	0.13	0.00	idem
28	Ni I	2	3.57	0.28	-2.68	-0.10				idem
38	Sr II	1	-1.02		-3.92	-1.34	-0.94		-1.26	syn
56	Ba II	1	-2.38		-4.51	-1.93	-2.22		-1.77	syn

Table A.1. continued.

Z	Atom	N_l	LTE				NLTE			Method of analysis
			$\log \varepsilon$	$\sigma_{\log \varepsilon}$	[X/H]	[X/Fe]	$\log \varepsilon$	$\sigma_{\log \varepsilon}$	[X/Fe]	
Milky Way comparison sample										
HD 2796, $T_{\text{eff}} = 4880$ K, $\log g = 1.55$, $[\text{Fe}/\text{H}] = -2.32$, $\xi_t = 1.8$ km s $^{-1}$										
11	Na I	2	4.22	0.02	-2.11	0.21	3.62	0.01	-0.39	syn
12	Mg I	4	5.54	0.05	-2.04	0.28	5.55	0.03	0.29	idem
13	Al I	1	3.54		-2.93	-0.61	3.65		-0.50	idem
14	Si I	1	5.43		-2.12	0.20	5.39		0.16	idem
20	Ca I	13	4.21	0.07	-2.15	0.17	4.36	0.08	0.31	idem
22	Ti I	11	2.65	0.06	-2.28	0.04	2.89	0.06	0.28	idem
22	Ti II	14	2.82	0.06	-2.11	0.21	2.83	0.05	0.22	idem
26	Fe I	45	5.00	0.08	-2.50	-0.18	5.13	0.07	-0.05	idem
26	Fe II	6	5.18	0.03	-2.32	0.00	5.18	0.03	0.00	idem
28	Ni I	2	3.73	0.05	-2.52	-0.20				idem
38	Sr II	2	0.55	0.01	-2.35	-0.03	0.57	0.05	-0.01	idem
56	Ba II	2	-0.46	0.07	-2.59	-0.27	-0.49	0.00	-0.30	idem
63	Eu II	1	-1.87		-2.38	-0.06	-1.80		0.01	idem
HD 4306, $T_{\text{eff}} = 4960$ K, $\log g = 2.18$, $[\text{Fe}/\text{H}] = -2.74$, $\xi_t = 1.3$ km s $^{-1}$										
11	Na I	2	3.99	0.01	-2.34	0.40	3.46	0.03	-0.13	syn
12	Mg I	4	5.27	0.02	-2.31	0.43	5.30	0.06	0.46	idem
13	Al I	1	3.20		-3.27	-0.53	3.42		-0.31	idem
14	Si I	1	5.28		-2.27	0.47	5.23		0.42	idem
20	Ca I	13	3.98	0.07	-2.38	0.36	4.11	0.07	0.49	idem
22	Ti I	8	2.41	0.02	-2.52	0.22	2.63	0.02	0.44	idem
22	Ti II	11	2.58	0.05	-2.35	0.39	2.59	0.05	0.40	idem
26	Fe I	45	4.60	0.09	-2.90	-0.16	4.71	0.09	-0.05	idem
26	Fe II	6	4.76	0.06	-2.74	0.00	4.76	0.06	0.00	idem
28	Ni I	2	3.32	0.05	-2.93	-0.19				idem
38	Sr II	2	0.17	0.01	-2.73	0.01	0.13	0.01	-0.03	idem
56	Ba II	1	-1.62		-3.75	-1.01	-1.62		-1.01	idem
HD 8724, $T_{\text{eff}} = 4560$ K, $\log g = 1.29$, $[\text{Fe}/\text{H}] = -1.76$, $\xi_t = 1.5$ km s $^{-1}$										
11	Na I	4	4.38	0.10	-1.95	-0.19	4.24	0.05	-0.33	syn
12	Mg I	2	6.24	0.04	-1.34	0.42	6.08	0.04	0.26	idem
20	Ca I	9	4.86	0.08	-1.50	0.26	4.93	0.09	0.33	idem
22	Ti I	8	3.09	0.09	-1.84	-0.08	3.30	0.07	0.13	idem
22	Ti II	12	3.38	0.04	-1.55	0.21	3.38	0.04	0.21	idem
26	Fe I	32	5.63	0.10	-1.87	-0.11	5.70	0.10	-0.04	idem
26	Fe II	5	5.74	0.04	-1.76	0.00	5.74	0.04	0.00	idem
28	Ni I	2	4.34	0.16	-1.91	-0.15				idem
38	Sr II	1	1.10		-1.80	-0.04	1.18		0.04	idem
56	Ba II	2	0.58	0.07	-1.55	0.21	0.44	0.01	0.07	idem
63	Eu II	1	-1.03		-1.54	0.22	-0.97		0.28	idem
HD 108317, $T_{\text{eff}} = 5270$ K, $\log g = 2.96$, $[\text{Fe}/\text{H}] = -2.18$, $\xi_t = 1.2$ km s $^{-1}$										
11	Na I	2	4.41	0.06	-1.92	0.26	3.85	0.06	-0.30	syn
12	Mg I	3	5.67	0.04	-1.91	0.27	5.65	0.01	0.25	idem
20	Ca I	12	4.46	0.06	-1.90	0.28	4.51	0.09	0.33	idem
22	Ti I	9	2.90	0.03	-2.03	0.15	3.03	0.04	0.28	idem
22	Ti II	8	3.04	0.03	-1.89	0.29	3.05	0.03	0.30	idem
26	Fe I	45	5.19	0.17	-2.31	-0.13	5.25	0.17	-0.07	idem
26	Fe II	6	5.32	0.05	-2.18	0.00	5.32	0.05	0.00	idem
28	Ni I	2	3.91	0.08	-2.34	-0.16				idem
38	Sr II	2	0.80	0.05	-2.10	0.08	0.76	0.03	0.04	idem
56	Ba II	2	0.05	0.05	-2.08	0.10	0.03	0.02	0.08	idem
63	Eu II	1	-1.18		-1.69	0.49	-1.08		0.59	idem
HD 122563, $T_{\text{eff}} = 4600$ K, $\log g = 1.32$, $[\text{Fe}/\text{H}] = -2.61$, $\xi_t = 1.7$ km s $^{-1}$										
11	Na I	2	3.76	0.04	-2.57	0.06	3.34	0.04	-0.36	syn
12	Mg I	4	5.24	0.03	-2.34	0.29	5.28	0.03	0.33	idem
13	Al I	1	3.26		-3.21	-0.58	3.29		-0.55	idem
14	Si I	1	5.28		-2.27	0.36	5.25		0.33	idem
20	Ca I	12	3.84	0.06	-2.52	0.11	4.10	0.07	0.37	idem
22	Ti I	9	2.24	0.02	-2.69	-0.06	2.48	0.02	0.18	idem

Table A.1. continued.

Z	Atom	N_l	LTE				NLTE			Method of analysis
			$\log \varepsilon$	$\sigma_{\log \varepsilon}$	[X/H]	[X/Fe]	$\log \varepsilon$	$\sigma_{\log \varepsilon}$	[X/Fe]	
22	Ti II	13	2.52	0.06	-2.41	0.22	2.54	0.06	0.24	idem
26	Fe I	39	4.70	0.07	-2.80	-0.17	4.82	0.07	-0.05	idem
26	Fe II	4	4.87	0.03	-2.63	0.00	4.87	0.03	0.00	idem
28	Ni I	2	3.51	0.09	-2.74	-0.11				idem
38	Sr II	2	0.14	0.07	-2.76	-0.13	0.18	0.11	-0.09	idem
56	Ba II	2	-1.45	0.01	-3.58	-0.95	-1.37	0.01	-0.87	idem
63	Eu II	1	-2.80		-3.31	-0.68	-2.71		-0.59	idem
HD 128279, $T_{\text{eff}} = 5200$ K, $\log g = 3.00$, $[\text{Fe}/\text{H}] = -2.19$, $\xi_t = 1.1$ km s $^{-1}$										
11	Na I	2	4.23	0.03	-2.10	0.09	3.67	0.00	-0.47	syn
12	Mg I	4	5.68	0.04	-1.90	0.29	5.66	0.02	0.27	idem
13	Al I	1	3.59		-2.88	-0.69	3.82		-0.46	idem
14	Si I	1	5.52		-2.03	0.16	5.49		0.13	idem
20	Ca I	13	4.47	0.08	-1.89	0.30	4.51	0.10	0.34	idem
22	Ti I	8	2.90	0.01	-2.03	0.16	3.01	0.01	0.27	idem
22	Ti II	13	3.05	0.03	-1.88	0.31	3.05	0.03	0.31	idem
26	Fe I	45	5.22	0.17	-2.28	-0.09	5.26	0.17	-0.05	idem
26	Fe II	6	5.31	0.04	-2.19	0.00	5.31	0.04	0.00	idem
28	Ni I	2	3.97	0.08	-2.28	-0.09				idem
38	Sr II	2	0.36	0.03	-2.54	-0.35	0.32	0.01	-0.39	idem
56	Ba II	2	-0.46	0.04	-2.59	-0.40	-0.43	0.01	-0.37	idem
63	Eu II	1	-1.75		-2.26	-0.07	-1.65		0.03	idem
HD 218857, $T_{\text{eff}} = 5060$ K, $\log g = 2.53$, $[\text{Fe}/\text{H}] = -1.92$, $\xi_t = 1.4$ km s $^{-1}$										
11	Na I	2	4.48	0.05	-1.85	0.07	3.91	0.01	-0.50	syn
12	Mg I	3	5.84	0.06	-1.74	0.18	5.83	0.03	0.17	idem
20	Ca I	12	4.64	0.06	-1.72	0.20	4.68	0.08	0.24	idem
22	Ti I	8	3.12	0.03	-1.81	0.11	3.25	0.04	0.24	idem
22	Ti II	10	3.28	0.03	-1.65	0.27	3.28	0.03	0.27	idem
26	Fe I	45	5.47	0.17	-2.03	-0.11	5.52	0.17	-0.05	idem
26	Fe II	6	5.58	0.05	-1.92	0.00	5.58	0.05	0.00	idem
28	Ni I	2	4.14	0.16	-2.11	-0.19				idem
56	Ba II	2	-0.14	0.05	-2.27	-0.35	-0.20	0.05	-0.41	idem
BD -11° 0145, $T_{\text{eff}} = 4900$ K, $\log g = 1.73$, $[\text{Fe}/\text{H}] = -2.18$, $\xi_t = 1.8$ km s $^{-1}$										
11	Na I	2	4.41	0.01	-1.92	0.26	3.83	0.04	-0.32	syn
12	Mg I	4	5.70	0.05	-1.88	0.30	5.70	0.04	0.30	idem
13	Al I	1	3.61		-2.86	-0.68	3.74		-0.55	idem
14	Si I	1	5.50		-2.05	0.13	5.46		0.09	idem
20	Ca I	13	4.39	0.08	-1.97	0.21	4.50	0.09	0.32	idem
22	Ti I	10	2.85	0.06	-2.08	0.10	3.07	0.07	0.32	idem
22	Ti II	15	3.03	0.05	-1.90	0.28	3.03	0.05	0.28	idem
26	Fe I	40	5.17	0.09	-2.33	-0.15	5.26	0.09	-0.06	idem
26	Fe II	5	5.32	0.04	-2.18	0.00	5.32	0.04	0.00	idem
28	Ni I	2	3.86	0.05	-2.39	-0.21				idem
38	Sr II	2	0.82	0.03	-2.08	0.10	0.84	0.05	0.12	idem
56	Ba II	2	0.26	0.14	-1.87	0.31	0.10	0.01	0.15	idem
63	Eu II	1	-1.29		-1.80	0.38	-1.21		0.46	idem
CD -24° 1782, $T_{\text{eff}} = 5140$ K, $\log g = 2.62$, $[\text{Fe}/\text{H}] = -2.72$, $\xi_t = 1.2$ km s $^{-1}$										
11	Na I	2	3.89	0.08	-2.44	0.28	3.34	0.04	-0.27	syn
12	Mg I	3	5.29	0.01	-2.29	0.43	5.29	0.01	0.43	idem
20	Ca I	12	3.94	0.09	-2.42	0.30	4.04	0.08	0.40	idem
22	Ti I	9	2.46	0.04	-2.47	0.25	2.64	0.04	0.43	idem
22	Ti II	8	2.53	0.02	-2.40	0.32	2.54	0.02	0.33	idem
26	Fe I	47	4.68	0.16	-2.82	-0.10	4.77	0.16	-0.01	idem
26	Fe II	6	4.78	0.05	-2.72	0.00	4.78	0.05	0.00	idem
28	Ni I	2	3.46	0.07	-2.79	-0.07				idem
38	Sr II	2	0.20	0.00	-2.70	0.02	0.18	0.03	0.00	idem
56	Ba II	1	-1.18		-3.31	-0.59	-1.09		-0.50	idem
BS16550-087, $T_{\text{eff}} = 4750$ K, $\log g = 1.5$, $[\text{Fe}/\text{H}] = -3.40$, $\xi_t = 2.0$ km s $^{-1}$										
11	Na I	2	2.67	0.05	-3.66	-0.26	2.60	0.00	-0.33	$W_{\text{obs}}(\text{CCT13})$
12	Mg I	6	4.66	0.04	-2.92	0.48	4.75	0.12	0.57	idem

Table A.1. continued.

Z	Atom	N_l	LTE				NLTE			Method of analysis
			$\log \varepsilon$	$\sigma_{\log \varepsilon}$	[X/H]	[X/Fe]	$\log \varepsilon$	$\sigma_{\log \varepsilon}$	[X/Fe]	
13	Al I	1	2.51		-3.96	-0.56	2.83		-0.24	idem
14	Si I	1	4.48		-3.07	0.33	4.42		0.27	idem
20	Ca I	6	3.09	0.04	-3.27	0.13	3.32	0.05	0.36	idem
22	Ti I	6	1.55	0.04	-3.38	0.02	1.83	0.04	0.30	idem
22	Ti II	16	1.65	0.11	-3.28	0.12	1.65	0.13	0.12	idem
26	Fe I	42	3.90	0.09	-3.60	-0.20	4.14	0.09	0.04	idem
26	Fe II	12	4.10	0.14	-3.40	0.00	4.10	0.14	0.00	idem
28	Ni I	2	2.51	0.05	-3.74	-0.34				idem
38	Sr II	1	0.02		-2.88	0.52	-0.04		0.46	idem
56	Ba II	1	-2.26		-4.39	-0.99	-2.06		-0.79	idem
HE0011-0035, $T_{\text{eff}} = 4950$ K, $\log g = 2.0$, $[\text{Fe}/\text{H}] = -3.04$, $\xi_t = 2.0$ km s ⁻¹										
12	Mg I	4	5.03	0.13	-2.55	0.49	5.11	0.23	0.57	W_{obs} (CCT13)
13	Al I	1	2.68		-3.79	-0.75	3.05		-0.38	idem
14	Si I	1	5.04		-2.51	0.53	4.99		0.48	idem
20	Ca I	4	3.63	0.08	-2.73	0.31	3.82	0.05	0.50	idem
22	Ti I	5	2.16	0.10	-2.77	0.27	2.41	0.10	0.52	idem
22	Ti II	14	2.31	0.23	-2.62	0.42	2.32	0.25	0.43	idem
26	Fe I	38	4.32	0.20	-3.18	-0.14	4.44	0.21	-0.02	idem
26	Fe II	11	4.46	0.15	-3.04	0.00	4.46	0.15	0.00	idem
28	Ni I	2	2.88	0.22	-3.37	-0.33				idem
38	Sr II	2	-0.69	0.08	-3.59	-0.55	-0.70	0.08	-0.56	syn
56	Ba II	1	-1.08		-3.21	-0.17	-1.04		-0.13	W_{obs} (CCT13)
63	Eu II	2	-1.69	0.09	-2.20	0.84	-1.54	0.05	0.99	idem
HE0039-4154, $T_{\text{eff}} = 4780$ K, $\log g = 1.6$, $[\text{Fe}/\text{H}] = -3.26$, $\xi_t = 2.0$ km s ⁻¹										
11	Na I	2	3.25	0.01	-3.08	0.18	2.90	0.06	-0.17	W_{obs} (CCT13)
12	Mg I	5	4.75	0.12	-2.83	0.43	4.83	0.22	0.51	idem
13	Al I	1	2.57		-3.90	-0.64	2.85		-0.36	idem
14	Si I	1	4.79		-2.76	0.50	4.73		0.44	idem
20	Ca I	5	3.20	0.10	-3.16	0.10	3.42	0.06	0.32	idem
22	Ti I	4	1.61	0.15	-3.32	-0.06	1.91	0.17	0.24	idem
22	Ti II	12	1.79	0.14	-3.14	0.12	1.81	0.15	0.14	idem
26	Fe I	41	4.11	0.21	-3.39	-0.13	4.30	0.22	0.06	idem
26	Fe II	7	4.24	0.18	-3.26	0.00	4.24	0.18	0.00	idem
28	Ni I	1	2.45		-3.80	-0.54				idem
38	Sr II	2	-0.81	0.07	-3.71	-0.45	-0.79	0.10	-0.43	syn
56	Ba II	3	-1.05	0.12	-3.18	0.08	-0.98	0.12	0.15	W_{obs} (CCT13)
63	Eu II	2	-2.59	0.09	-3.10	0.16	-2.39	0.05	0.36	idem
HE0048-0611, $T_{\text{eff}} = 5180$ K, $\log g = 2.70$, $[\text{Fe}/\text{H}] = -2.69$, $\xi_t = 1.7$ km s ⁻¹										
11	Na I	2	3.74	0.04	-2.59	0.10	3.37	0.10	-0.27	W_{obs} (CCT13)
12	Mg I	5	5.29	0.13	-2.29	0.40	5.33	0.17	0.44	idem
13	Al I	1	2.97		-3.50	-0.81	3.32		-0.46	idem
20	Ca I	5	3.99	0.11	-2.37	0.32	4.10	0.09	0.43	idem
22	Ti I	8	2.54	0.09	-2.39	0.30	2.72	0.09	0.48	idem
22	Ti II	16	2.71	0.13	-2.22	0.47	2.71	0.14	0.47	idem
26	Fe I	43	4.75	0.14	-2.75	-0.06	4.84	0.14	0.03	idem
26	Fe II	12	4.81	0.10	-2.69	0.00	4.81	0.10	0.00	idem
28	Ni I	3	3.37	0.18	-2.88	-0.19				idem
38	Sr II	1	0.28		-2.62	0.07	0.16		-0.05	idem
56	Ba II	1	-0.78		-2.91	-0.22	-0.69		-0.13	idem
HE0122-1616, $T_{\text{eff}} = 5200$ K, $\log g = 2.65$, $[\text{Fe}/\text{H}] = -2.85$, $\xi_t = 1.8$ km s ⁻¹										
11	Na I	2	3.23	0.04	-3.10	-0.25	3.02	0.11	-0.46	W_{obs} (CCT13)
12	Mg I	5	5.00	0.11	-2.58	0.27	5.06	0.17	0.33	idem
20	Ca I	5	3.68	0.03	-2.68	0.17	3.81	0.04	0.30	idem
22	Ti I	5	2.18	0.12	-2.75	0.10	2.39	0.11	0.31	idem
22	Ti II	10	2.23	0.11	-2.70	0.15	2.23	0.12	0.15	idem
26	Fe I	40	4.54	0.13	-2.96	-0.11	4.65	0.15	0.00	idem
26	Fe II	11	4.65	0.09	-2.85	0.00	4.65	0.09	0.00	idem
28	Ni I	2	3.09	0.13	-3.16	-0.31				idem
38	Sr II	1	-0.31		-3.21	-0.36	-0.36		-0.41	idem

Table A.1. continued.

Z	Atom	N_l	LTE				NLTE			Method of analysis
			$\log \varepsilon$	$\sigma_{\log \varepsilon}$	[X/H]	[X/Fe]	$\log \varepsilon$	$\sigma_{\log \varepsilon}$	[X/Fe]	
56	Ba II	1	-1.74		-3.87	-1.02	-1.58		-0.86	idem
HE0332-1007, $T_{\text{eff}} = 4750$ K, $\log g = 1.5$, $[\text{Fe}/\text{H}] = -2.89$, $\xi_t = 2.0$ km s ⁻¹										
11	Na I	2	3.48	0.02	-2.85	0.04	3.13	0.04	-0.31	W_{obs} (CCT13)
12	Mg I	5	5.03	0.07	-2.55	0.34	5.08	0.09	0.39	idem
13	Al I	1	3.08		-3.39	-0.50	3.16		-0.42	idem
14	Si I	1	4.90		-2.65	0.24	4.85		0.19	idem
20	Ca I	7	3.59	0.08	-2.77	0.12	3.78	0.04	0.31	idem
22	Ti I	5	2.09	0.07	-2.84	0.05	2.31	0.05	0.27	idem
22	Ti II	9	2.41	0.12	-2.52	0.37	2.38	0.13	0.34	idem
26	Fe I	41	4.45	0.15	-3.05	-0.16	4.59	0.15	-0.02	idem
26	Fe II	12	4.61	0.09	-2.89	0.00	4.61	0.09	0.00	idem
28	Ni I	2	3.22	0.12	-3.03	-0.14				idem
38	Sr II	2	-0.70	0.11	-3.60	-0.71	-0.71	0.11	-0.72	idem
56	Ba II	3	-1.07	0.09	-3.20	-0.31	-1.01	0.07	-0.25	idem
63	Eu II	3	-1.91	0.20	-2.42	0.47	-1.74	0.16	0.64	idem
HE0445-2339, $T_{\text{eff}} = 5165$ K, $\log g = 2.20$, $[\text{Fe}/\text{H}] = -2.76$, $\xi_t = 1.9$ km s ⁻¹										
11	Na I	2	3.50	0.14	-2.83	-0.07	3.24	0.07	-0.33	W_{obs} (CCT13)
12	Mg I	6	4.96	0.09	-2.62	0.14	5.05	0.13	0.23	idem
13	Al I	1	2.72		-3.75	-0.99	3.25		-0.46	idem
14	Si I	1	4.85		-2.70	0.06	4.81		0.02	idem
20	Ca I	6	3.70	0.05	-2.66	0.10	3.89	0.04	0.29	idem
22	Ti I	9	2.29	0.06	-2.64	0.12	2.58	0.05	0.41	idem
22	Ti II	18	2.41	0.10	-2.52	0.24	2.43	0.10	0.26	idem
26	Fe I	41	4.57	0.09	-2.93	-0.17	4.74	0.09	0.00	idem
26	Fe II	13	4.74	0.06	-2.76	0.00	4.74	0.06	0.00	idem
28	Ni I	3	3.24	0.09	-3.01	-0.25				idem
38	Sr II	1	0.21		-2.69	0.07	0.09		-0.05	idem
56	Ba II	1	-1.22		-3.35	-0.59	-1.06		-0.43	idem
HE1356-0622, $T_{\text{eff}} = 4945$ K, $\log g = 2.0$, $[\text{Fe}/\text{H}] = -3.45$, $\xi_t = 2.0$ km s ⁻¹										
11	Na I	2	3.15	0.04	-3.18	0.27	2.96	0.11	0.08	W_{obs} (CCT13)
12	Mg I	4	4.44	0.10	-3.14	0.31	4.55	0.22	0.42	idem
13	Al I	1	2.11		-4.36	-0.91	2.69		-0.33	idem
14	Si I	1	4.60		-2.95	0.50	4.55		0.45	idem
20	Ca I	4	3.23	0.10	-3.13	0.32	3.44	0.08	0.53	idem
22	Ti I	4	1.72	0.05	-3.21	0.24	2.03	0.03	0.55	idem
22	Ti II	12	1.72	0.10	-3.21	0.24	1.75	0.10	0.27	idem
26	Fe I	35	3.81	0.11	-3.69	-0.24	4.01	0.12	-0.04	idem
26	Fe II	8	4.05	0.08	-3.45	0.00	4.05	0.08	0.00	idem
28	Ni I	2	2.43	0.10	-3.82	-0.37				idem
38	Sr II	2	-2.51	0.07	-5.41	-1.96	-2.26	0.10	-1.71	idem
56	Ba II	1	-2.41		-4.54	-1.09	-2.21		-0.89	idem
HE1357-0123, $T_{\text{eff}} = 4600$ K, $\log g = 1.2$, $[\text{Fe}/\text{H}] = -3.92$, $\xi_t = 2.1$ km s ⁻¹										
11	Na I	2	2.81	0.10	-3.52	0.40	2.70	0.03	0.29	W_{obs} (CCT13)
12	Mg I	3	4.17	0.17	-3.41	0.51	4.28	0.43	0.62	idem
13	Al I	1	1.74		-4.73	-0.81	2.21		-0.34	idem
14	Si I	1	3.91		-3.64	0.28	3.86		0.23	idem
20	Ca I	3	2.86	0.08	-3.50	0.42	3.13	0.03	0.69	idem
22	Ti I	3	1.18	0.26	-3.75	0.17	1.60	0.24	0.59	idem
22	Ti II	11	1.20	0.14	-3.73	0.19	1.28	0.13	0.27	idem
26	Fe I	36	3.47	0.14	-4.03	-0.11	3.76	0.17	0.18	idem
26	Fe II	6	3.58	0.09	-3.92	0.00	3.58	0.09	0.00	idem
28	Ni I	1	1.87		-4.38	-0.46				idem
38	Sr II	2	-3.38	0.30	-6.28	-2.36	-3.05	0.25	-2.03	idem
HE1416-1032, $T_{\text{eff}} = 5000$ K, $\log g = 2.0$, $[\text{Fe}/\text{H}] = -3.23$, $\xi_t = 2.1$ km s ⁻¹										
12	Mg I	5	4.40	0.08	-3.18	0.05	4.52	0.13	0.17	W_{obs} (CCT13)
13	Al I	1	2.13		-4.34	-1.11	2.73		-0.51	idem
14	Si I	1	4.36		-3.19	0.04	4.32		0.00	idem
20	Ca I	4	3.12	0.03	-3.24	-0.01	3.33	0.05	0.20	idem
22	Ti I	3	1.74	0.07	-3.19	0.04	2.05	0.07	0.35	idem

Table A.1. continued.

Z	Atom	N_l	LTE				NLTE			Method of analysis
			$\log \varepsilon$	$\sigma_{\log \varepsilon}$	[X/H]	[X/Fe]	$\log \varepsilon$	$\sigma_{\log \varepsilon}$	[X/Fe]	
22	Ti II	11	1.87	0.10	-3.06	0.17	1.89	0.10	0.19	idem
26	Fe I	41	4.08	0.13	-3.42	-0.19	4.25	0.14	-0.02	idem
26	Fe II	8	4.27	0.11	-3.23	0.00	4.27	0.11	0.00	idem
28	Ni I	2	2.87	0.11	-3.38	-0.15				idem
38	Sr II	2	-2.12	0.05	-5.02	-1.79	-1.84	0.02	-1.51	idem
56	Ba II	1	-2.33		-4.46	-1.23	-2.12		-1.02	idem
HE2244-2116, $T_{\text{eff}} = 5230$ K, $\log g = 2.80$, $[\text{Fe}/\text{H}] = -2.40$, $\xi_t = 1.7$ km s ⁻¹										
11	Na I	2	4.12	0.01	-2.21	0.19	3.67	0.06	-0.26	W_{obs} (CCT13)
12	Mg I	5	5.53	0.15	-2.05	0.35	5.56	0.17	0.38	idem
13	Al I	1	3.54		-2.93	-0.53	3.83		-0.24	idem
20	Ca I	9	4.24	0.06	-2.12	0.28	4.33	0.07	0.37	idem
22	Ti I	9	2.81	0.11	-2.12	0.28	2.97	0.11	0.44	idem
22	Ti II	18	3.00	0.08	-1.93	0.47	2.99	0.09	0.46	idem
26	Fe I	41	5.05	0.11	-2.45	-0.05	5.12	0.12	0.02	idem
26	Fe II	12	5.10	0.06	-2.40	0.00	5.10	0.06	0.00	idem
28	Ni I	3	3.78	0.21	-2.47	-0.07				idem
38	Sr II	1	0.44		-2.46	-0.06	0.32		-0.18	idem
56	Ba II	1	-0.20		-2.33	0.07	-0.15		0.12	idem
63	Eu II	3	-1.12	0.23	-1.63	0.77	-1.00	0.21	0.89	idem
HE2249-1704, $T_{\text{eff}} = 4590$ K, $\log g = 1.2$, $[\text{Fe}/\text{H}] = -2.94$, $\xi_t = 2.0$ km s ⁻¹										
12	Mg I	4	4.82	0.03	-2.76	0.18	4.88	0.10	0.24	W_{obs} (CCT13)
13	Al I	1	2.76		-3.71	-0.77	2.89		-0.64	idem
14	Si I	1	4.81		-2.74	0.20	4.78		0.17	idem
20	Ca I	4	3.36	0.06	-3.00	-0.06	3.64	0.10	0.22	idem
22	Ti I	10	1.96	0.10	-2.97	-0.03	2.22	0.11	0.23	idem
22	Ti II	13	2.24	0.10	-2.69	0.25	2.24	0.10	0.25	idem
26	Fe I	28	4.46	0.14	-3.04	-0.10	4.58	0.14	0.02	idem
26	Fe II	12	4.56	0.07	-2.94	0.00	4.56	0.07	0.00	idem
28	Ni I	3	3.23	0.04	-3.02	-0.08				idem
38	Sr II	2	-2.15	0.09	-5.05	-2.11	-1.80	0.12	-1.76	idem
56	Ba II	1	-2.77		-4.90	-1.96	-2.56		-1.75	idem
HE2252-4225, $T_{\text{eff}} = 4750$ K, $\log g = 1.55$, $[\text{Fe}/\text{H}] = -2.76$, $\xi_t = 1.9$ km s ⁻¹										
11	Na I	2	3.59	0.01	-2.74	0.02	3.15	0.01	-0.42	syn
12	Mg I	3	5.02	0.03	-2.56	0.20	5.12	0.09	0.30	idem
13	Al I	1	2.95		-3.52	-0.76	3.09		-0.62	idem
14	Si I	1	5.03		-2.52	0.24	5.01		0.22	idem
20	Ca I	9	3.71	0.05	-2.65	0.11	3.86	0.08	0.26	idem
22	Ti I	8	2.31	0.06	-2.62	0.14	2.54	0.05	0.37	idem
22	Ti II	13	2.58	0.05	-2.35	0.41	2.58	0.05	0.41	idem
26	Fe I	32	4.59	0.09	-2.91	-0.15	4.73	0.09	-0.01	idem
26	Fe II	8	4.74	0.07	-2.76	0.00	4.74	0.07	0.00	idem
28	Ni I	6	3.39	0.11	-2.86	-0.10				idem
38	Sr II	2	0.07	0.01	-2.83	-0.07	0.05	0.05	-0.09	idem
56	Ba II	3	-0.30	0.04	-2.43	0.33	-0.39	0.09	0.24	idem
63	Eu II	4	-1.35	0.02	-1.86	0.90	-1.25	0.02	1.00	idem
HE2327-5642, $T_{\text{eff}} = 5050$ K, $\log g = 2.20$, $[\text{Fe}/\text{H}] = -2.92$, $\xi_t = 1.7$ km s ⁻¹										
11	Na I	2	3.34	0.07	-2.99	-0.07	2.95	0.07	-0.46	syn
12	Mg I	3	4.87	0.03	-2.71	0.21	5.00	0.11	0.34	idem
13	Al I	1	2.54		-3.93	-1.01	3.02		-0.53	idem
14	Si I	1	4.88		-2.67	0.25	4.84		0.21	idem
20	Ca I	8	3.57	0.06	-2.79	0.13	3.70	0.06	0.26	idem
22	Ti I	10	2.07	0.06	-2.86	0.06	2.34	0.07	0.33	idem
22	Ti II	23	2.19	0.09	-2.74	0.18	2.21	0.09	0.20	idem
26	Fe I	33	4.45	0.10	-3.05	-0.13	4.59	0.09	0.01	idem
26	Fe II	7	4.58	0.06	-2.92	0.00	4.58	0.06	0.00	idem
28	Ni I	8	3.15	0.07	-3.10	-0.18				idem
38	Sr II	2	0.17	0.01	-2.73	0.19	0.04	0.01	0.06	idem
56	Ba II	3	-0.33	0.03	-2.46	0.46	-0.35	0.09	0.44	idem
63	Eu II	4	-1.32	0.02	-1.83	1.09	-1.22	0.02	1.19	idem

Table A.1. continued.

Z	Atom	N_l	LTE				NLTE			Method of analysis
			$\log \varepsilon$	$\sigma_{\log \varepsilon}$	[X/H]	[X/Fe]	$\log \varepsilon$	$\sigma_{\log \varepsilon}$	[X/Fe]	
Ref. CCT13 = Cohen et al. (2013), CH10= Cohen & Huang (2010), FNG16 = Frebel et al. (2016), FSG10 = Frebel et al. (2010), GNM13 = Gilmore et al. (2013), JNM15 = Jablonka et al. (2015), KC12 = Kirby & Cohen (2012), NYG10 = Norris et al. (2010), SFM10 = Simon et al. (2010), SJF15 = Simon et al. (2015), TJH10 = Tafelmeyer et al. (2010), UCK15 = Ural et al. (2015), syn = synthetic spectrum method.										

